Direct covariance measurement of CO_2 gas transfer velocity during the 2008 Southern Ocean Gas Exchange Experiment: Wind speed dependency

J. B. Edson,[1] C. W. Fairall,[2] L. Bariteau,[3] C. J. Zappa,[4] A. Cifuentes-Lorenzen,[1] W. R. McGillis,[4] S. Pezoa,[2] J. E. Hare,[3] and D. Helmig[5]

Received 2 February 2011; revised 13 July 2011; accepted 12 August 2011; published 11 November 2011.

[1] Direct measurements of air-sea heat, momentum, and mass (including CO_2, DMS, and water vapor) fluxes using the direct covariance method were made over the open ocean from the NOAA R/V *Ronald H. Brown* during the Southern Ocean Gas Exchange (SO GasEx) program. Observations of fluxes and the physical processes associated with driving air-sea exchange are key components of SO GasEx. This paper focuses on the exchange of CO_2 and the wind speed dependency of the transfer velocity, k, used to model the CO_2 flux between the atmosphere and ocean. A quadratic dependence of k on wind speed based on dual tracer experiments is most frequently encountered in the literature. However, in recent years, bubble-mediated enhancement of k, which exhibits a cubic relationship with wind speed, has emerged as a key issue for flux parameterization in high-wind regions. Therefore, a major question addressed in SO GasEx is whether the transfer velocities obey a quadratic or cubic relationship with wind speed. After significant correction to the flux estimates (primarily due to moisture contamination), the direct covariance CO_2 fluxes confirm a significant enhancement of the transfer velocity at high winds compared with previous quadratic formulations. Regression analysis suggests that a cubic relationship provides a more accurate parameterization over a wind speed range of 0 to 18 m s^{-1}. The Southern Ocean results are in good agreement with the 1998 GasEx experiment in the North Atlantic and a recent separate field program in the North Sea.

Citation: Edson, J. B., C. W. Fairall, L. Bariteau, C. J. Zappa, A. Cifuentes-Lorenzen, W. R. McGillis, S. Pezoa, J. E. Hare, and D. Helmig (2011), Direct covariance measurement of CO_2 gas transfer velocity during the 2008 Southern Ocean Gas Exchange Experiment: Wind speed dependency, *J. Geophys. Res.*, *116*, C00F10, doi:10.1029/2011JC007022.

1. Introduction

[2] Air-sea fluxes of heat, momentum, moisture, and trace gases are critical components of the Earth's climate system. Carbon dioxide is the most prominent trace gas in this respect. Other gases that are exchanged between the atmosphere and the ocean, including methane, ozone, and dimethylsulfide (DMS) also contribute to the climate system and have further implications in ecosystems, pollution, and cloud dynamics. Direct measurements of air-sea energy fluxes in the last decades have led to substantial improvements in flux parameterizations with applications in numerical models and for estimating fluxes from measured bulk data. Research programs in climate, weather, and air pollution have prompted the need for global air-sea flux estimates with ever increasing demands for higher temporal and spatial resolution [see *Taylor*, 2000]. Thus, the development of methods for determination of ocean-atmosphere fluxes from satellites and implementation of these variables in regional and global air chemistry models have become a major research focus (see discussion by *Broadgate* [2004]). Substantial difficulties remain in parameterizing the gas/chemical transfer processes and in determining the relevant inputs from satellite measurements.

[3] The kinetics of air-sea gas exchange is not completely understood, and this lack of knowledge impedes our ability to accurately portray the local and regional flux of trace gases between the atmosphere and ocean. Gas transfer is a nonlinear process with complex dependencies in both the ocean and atmosphere. For gases with strong ocean molecular sublayer resistance (such as CO_2), the exchange is significantly increased with higher wind speeds, wave breaking, production of bubbles, and enhanced underwater turbulent processes. Although air-sea gas transfer is recognized to

[1]Department of Marine Sciences, University of Connecticut, Groton, Connecticut, USA.
[2]Earth System Research Laboratory, NOAA, Boulder, Colorado, USA.
[3]Cooperative Institute for Research in Environmental Sciences, University of Colorado at Boulder, Boulder, Colorado, USA.
[4]Lamont-Doherty Earth Observatory, Earth Institute at Columbia University, Palisades, New York, USA.
[5]Institute of Alpine and Arctic Research, University of Colorado at Boulder, Boulder, Colorado, USA.

0148-0227/11/2011JC007022

have a strong correlation with wind speed, other processes also play a role. For example, at low winds, surfactants, buoyancy, rain, microscale wave breaking, and biological productivity may significantly affect gas transfer.

[4] The last decade has seen significant progress in improving physical representations of gas transfer (see the review by *Wanninkhof et al.* [2009]). This progress relies on measurements of the air-sea flux of the gas with both indirect (tracer) and direct (direct covariance or eddy correlation) techniques. Examples of recent gas transfer field programs featuring direct covariance techniques from ships at sea include GasEx98 and GasEx01 [*McGillis et al.*, 2001a; *Hare et al.*, 2004] and North Atlantic cruises [*Miller et al.*, 2009, 2010; *Prytherch et al.*, 2010b]; for CO_2, for DMS [*Blomquist et al.*, 2006; *Marandino et al.*, 2009; *Miller et al.*, 2009], and for ozone [*Bariteau et al.*, 2010].

[5] While global fluxes are of primary interest, the flux data obtained in isolated field programs are principally used to characterize the local transfer through *the gas transfer velocity*. The expression of the air-sea flux, F_x, of a gas can be written in terms of the solubility (α_x) and air-sea partial pressure (fugacity, f_x) difference as:

$$F_x = k\,\alpha_x\,(f_{xw} - f_{xa}) \tag{1}$$

where the subscripts indicate "water" and "air" and k is the gas transfer velocity. There are many hidden details within this expression (e.g., see section 4). For CO_2, the most uncertain parameter in (1) is the transfer velocity. In the past, simple wind speed–dependent models for k were presented, such as that of *Liss and Merlivat* [1986] and *Wanninkhof* [1992], which were piecewise linear and quadratic with wind speed, respectively. Accurate estimation of the mean air-sea flux of carbon dioxide over any region of the ocean requires determination of the transfer velocity as well as the air-sea fugacity gradient on the time scale of the forcing mechanisms. That is, it is not sufficient to determine monthly averages of these quantities, due to the cross correlation between them at smaller time scales. By directly measuring the flux and the air-sea fugacity gradient, one can compute "observed" gas transfer velocities.

[6] Scientific knowledge gained by these field studies has promoted the development of physically based representations of k. For example, *Fairall et al.* [2000] took a micrometeorological approach to develop the Coupled Ocean Atmosphere Response Experiment Gas (COAREG) transfer model. In essence, the model describes the turbulent and molecular processes on both sides of the two-fluid interface; it incorporates the surface renewal concepts of *Soloviev and Schlüssel* [1994] and the empirical bubble enhancement model of *Woolf* [1997]. Furthermore, this parameterization describes the flux on the scale (subhour) of the physical processes which drive the gas transfer. The model has recently been extended to DMS [*Blomquist et al.*, 2006] and gases such as ozone that are destroyed by chemical reactions after deposition to the ocean surface [*Fairall et al.*, 2007]. *Soloviev* [2007] has developed a similar model that also includes surface wave effects.

[7] Reconciliation of the new data sets with advances in theory discussed above highlights the necessity for more observations of open ocean flux of CO_2 and other gases in conjunction with further investigation of the surface processes which drive air-sea gas transfer. The emergence of bubble-mediated transfer as a key issue in high-wind regions led to the identification of the Southern Ocean as a top priority for a new study of gas transfer processes. Due to differences in solubility effects at higher winds, the observation of the transfer of multiple gases permits the differentiation between bubble, ocean turbulent, and atmospheric turbulent components of the transfer. Thus, the 2008 Southern Ocean GasEx (SO GasEx) field program was born [*Ho et al.*, 2011a].

[8] One key component of SO GasEx was observations of trace gas fluxes and the physical processes associated with driving those fluxes. This work was done by the (informal) direct covariance and surface processes group (DCSPG). The group performed measurements of the flux of CO_2, DMS, ozone, momentum, moisture, and sensible heat plus the bulk meteorological and chemical variables for the computation of transfer coefficients. Surface properties such as waves, wave breaking statistics, oceanic turbulence, and bubbles were also made using heave corrected laser and microwave altimeters, high-resolution cameras, a drifting buoy, and a Wave and Surface Current Monitoring System (WaMoS) that used the ship's radar.

[9] Direct covariance results have already been reported for DMS [*Blomquist et al*., 2010; *Yang et al.*, 2011] and ozone [*Bariteau et al.*, 2010; D. Helmig et al., Atmosphere-ocean ozone fluxes during the TexAQS 2006, STRATUS 2006, GOMECC 2007, GasEx 2008, and AMMA 2008 cruises, submitted to *Journal of Geophysical Research*, 2011]. Improvements to the COAREG bulk flux algorithm for DMS, CO_2 and ozone based on SO GasEx and these studies are described by *Fairall et al.* [2011]. Investigations of the transfer coefficients using the dual tracer techniques are given by *Ho et al.* [2011b]. This paper provides an analysis of the CO_2 flux and reports the wind speed dependence of the CO_2 transfer coefficient. Following this introduction, a short description of SO GasEx is given. Measurement details are given in section 3 and the CO_2 transfer coefficients are presented in section 4. Further discussion of the transfer velocity results is presented in section 5 and conclusions are given in section 6.

2. Background on Southern Ocean GasEx

[10] GasEx is a U.S.-led series of cruises to use process studies to improve quantification of air-sea CO_2 fluxes and the gas transfer velocity initiated in 1998. So far, three large-scale studies have been conducted, one in the North Atlantic (GasEx-98), one in the Equatorial Pacific (GasEx-01), and one in the Southern Ocean (SO GasEx). One of the main goals of these efforts is to quantify transfer velocities on a regional scale from remote sensing such that, combined with regional ΔpCO_2, global air-sea CO_2 fluxes can be determined. A systematic approach is followed to accomplish this goal that involves the following steps: (1) make direct flux measurements in the field to obtain short-term local CO_2 fluxes and gas transfer velocities, (2) reconcile direct CO_2 flux measurement with integrated measurements of gas transfer velocities using the $^3He/SF_6$ dual tracer technique, (3) understand the mechanisms controlling ocean mixed layer pCO_2 on short time and space scales, (4) elucidate the forcing functions controlling gas transfer, and (5) relate

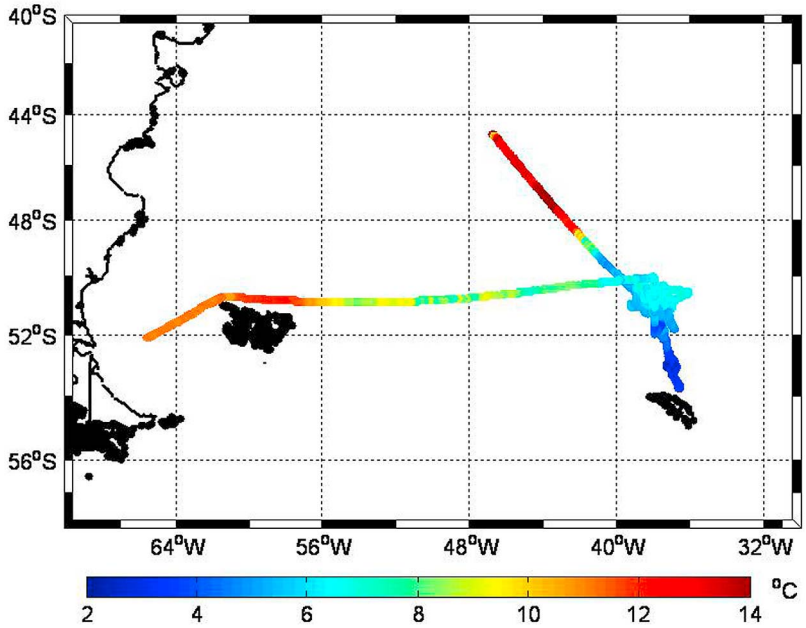

Figure 1. Cruise track for SO GasEx, which starts in Punta Arenas, Chile, and ends during the transect to Uruguay. The color denotes the sea surface temperature values shown in the color bar.

forcing functions to parameters that can be detected by remote sensing.

[11] SO GasEx was conceived to address observational gaps remaining from the first two experiments: principally to examine processes at higher wind speeds, to obtain data in a previously unexplored region, and to take advantage of technological advances to expand the information on forcing of exchange processes. Some eleven research groups participated with studies of direct tracers, direct covariance fluxes, autonomous buoys, ocean mixing, nutrients, colored dissolved organic matter (CDOM), dissolved organics, optical properties, optical scattering mechanisms, and phytoplankton. An overall description of SO GasEx is provided by *Ho et al.* [2011a].

[12] The cruise was conducted on the NOAA R/V *Ronald H. Brown*, which departed southern Chile on 28 February 2008, spent 37 days at or near the primary observation area at 51°S, 36°N, finally arriving in Uruguay on 9 April 2008. The cruise track for the experiment is shown in Figure 1. This location was chosen as a compromise between the need for both high wind speeds and large ΔpCO_2. Time series of several pertinent meteorological and oceanic variables are shown in Figure 2. Time series of the momentum (i.e., surface stress), sensible heat and latent heat fluxes computed using the COARE 3.0 algorithm [*Fairall et al.*, 2003] are shown in Figure 3, along with directly measured downwelling and parameterized upwelling radiative fluxes. The measured transfer coefficients for momentum (i.e., the Drag Coefficient) and latent heat were very similar to the nominal ocean values used in the COARE algorithm [*Fairall et al.*, 2011]. The mean 10 m wind speed during the experiment was 9.7 m s^{-1} the standard deviation was 3.2 m s^{-1}. Winds speeds reached a maximum of 20.7 m s^{-1} during the transit back to Uruguay. The mean relative humidity was 87% and the median was 90%. More than 25% of observations exceeded 96% relative humidity which is on the edge of reliable *RH* measurements from the sensors used. The mean sea-air temperature difference was essentially zero and positive and negative values were about equally probable with 75% of observations within 2.0 C of neutral. Cloud, rainy conditions with high humidity were common. A total of 185 mm of rain was measured.

3. Measurement Details

[13] The most accurate (and unbiased) technique for observation of the heat fluxes is the *direct covariance method*. In the case of heat fluxes, the procedure requires computation of the covariance of the fluctuations of wind vertical velocity with the measured perturbations of temperature (sensible heat), humidity (latent heat) or CO_2. However, on an oceangoing vessel, the measured wind speed fluctuations are contaminated by the platform response to the underlying waves, so it is necessary to accurately measure the ship's tilt angles and velocities at sampling frequencies comparable to the velocity measurements [*Edson et al.*, 1998]. This motion information is used to remove the platform velocities from the measured wind to arrive at the earth-referenced vertical velocity wind fluctuations.

[14] The fluxes and mean variables used in this analysis were obtained from the University of Connecticut (UConn) Direct Covariance Flux System (DCFS) [*Edson et al.*, 1998, 2004] and the NOAA/ESRL/PSD system [*Fairall et al.*, 2003, 2006]. A separate system for DMS flux measurements was also deployed [*Blomquist et al.*, 2010], but those observations are the focus of investigation reported by *Yang et al.* [2011] and are not part of this analysis. Comprehensive system descriptions are provided in previous publications, so only details specific to this field program will be provided here. Fast response velocity and temperature were obtained from Gill R-3 sonic anemometers, fast humidity from LI-6262 and LI-7500 IR absorption hygrometers, fast heading

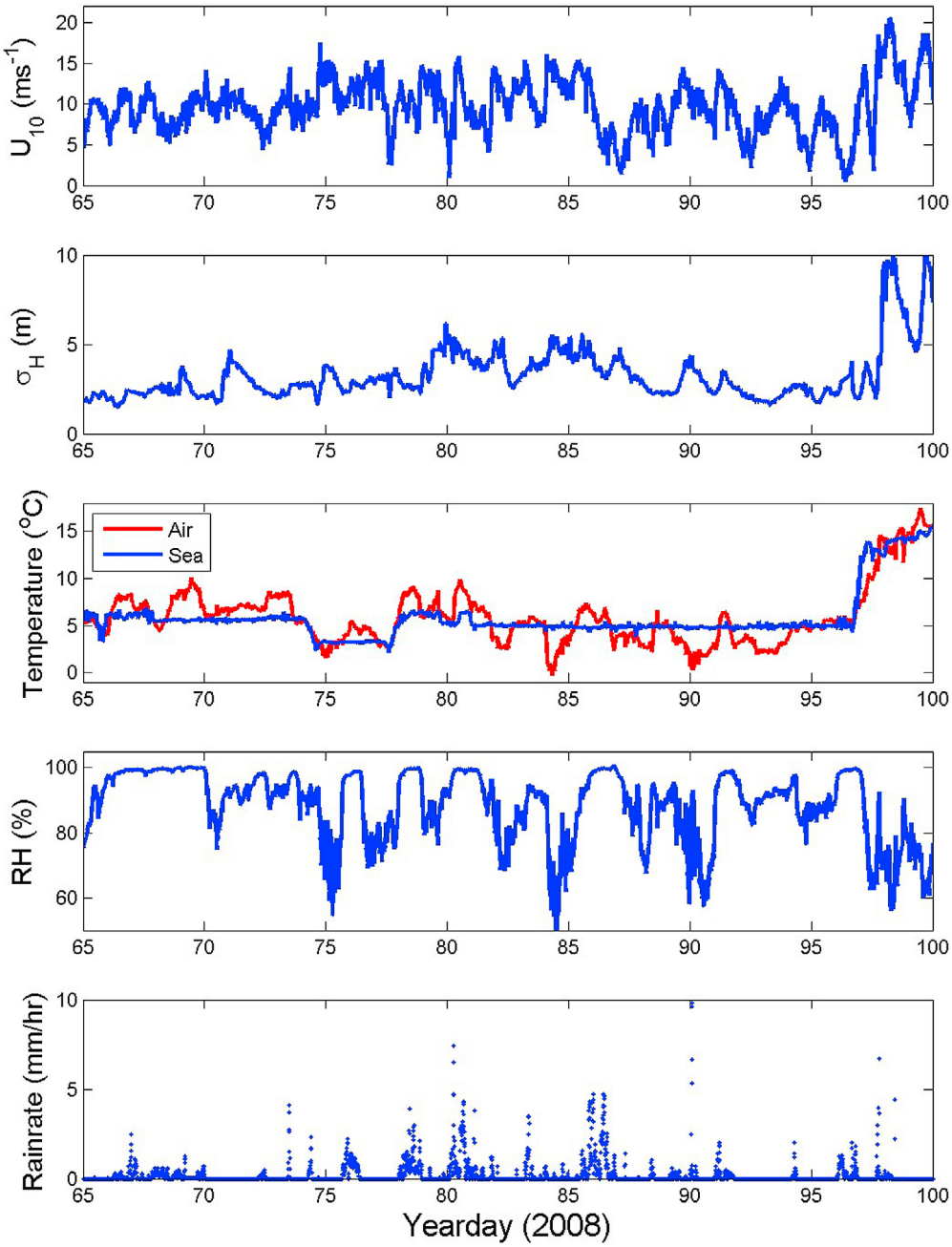

Figure 2. Time series of wind speed adjusted to 10 m, significant wave height, air and sea temperature, relative humidity, and rain rate for SO GasEx during March and April 2008. Yearday 65 is 5 March 2008, and yearday 100 is 10 April 2008.

from a GPS compass and ship motion corrections from Systron-Donner MotionPak six-variable (three-axis linear acceleration and three-axis angular velocity) motion packages integrated with the sonic anemometer mounts. Table 1 lists the main instrument types.

[15] Sonic anemometers/thermometers with motion correction packages were mounted on the jackstaff for SO GasEx as shown in Figure 4. The central sonic anemometer was positioned 1.6 m forward of the main mast and the anemometers were approximately 18 m above the ocean surface. Flow distortion between instruments was minimized by limiting the relative wind directions used in our analyses. For example, the relative wind directions were limited to −90° (from port to starboard in the coordinate system used in this analysis) to 50° of bow-on for the portside sonic used to compute the CO_2 fluxes for this investigation. An empirical correction for flow distortion due to the ship's superstructure was applied to the sonic anemometers based on previous flow distortion studies [*Fairall et al.*, 2003; *Dupuis et al.*, 2003].

[16] Closed path nondispersive infrared (NDIR) gas analyzers such as the LI-6262 require drawing a sample of air through a tube into the detector cell of the instrument. Using this strategy, some reduction in signal is expected for higher

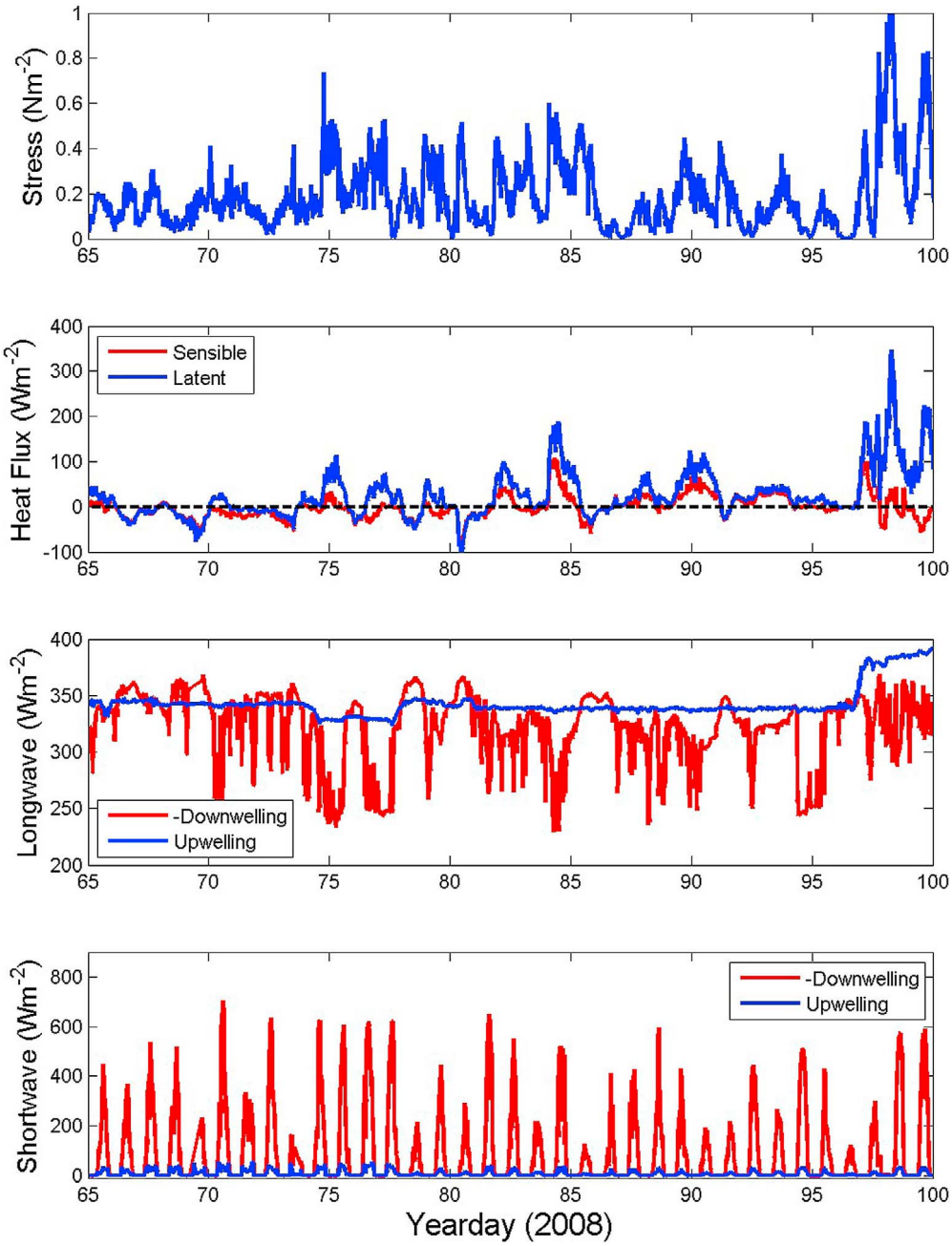

Figure 3. Flux time series of surface stress, sensible and latent heat flux, downwelling and upwelling longwave (IR) radiative flux, and downwelling and upwelling shortwave (solar) radiative flux. The first, second, and third panels are bulk fluxes computed using the COARE algorithm.

spectral frequencies, but contamination problems are greatly reduced. For the first two GasEx cruises, an innovative approach was undertaken [*McGillis et al.*, 2001a, 2001b], where improved closed path carbon dioxide measurement systems were deployed, and frequent "zero" calibrations were applied to account for platform effects. Accurate pumps, a pressure reservoir and thermal controls were incorporated into the sampling tube design, and the instrument was housed in a climate controlled chamber.

[17] Unfortunately, the removal of the forward scaffold on the R/V *Ronald H. Brown* led to much longer sampling tubes. In SO GasEx, the closed path sensors were mounted in a van on the O2 deck of the R/V *Ronald H. Brown* and air was drawn through approximately 25 m tubes. Subsequent analysis of these sensors revealed system noise that made these measurements unsuitable for flux estimates. The noise was very broadband in nature (i.e., it was not clearly identifiable with ship motion) and the cause remains unexplained after significant time and effort.

[18] Instead, SO GasEx relied on five LI-7500 open path NDIR analyzers mounted very close to the sonic anemometers as shown in Figure 4. Three of the open path NDIR analyzers were deployed near the portside sonic anemometer used in this analysis. These sensors were flushed at least once

Table 1. Measurement Systems From the Ship Eddy Covariance Group in GasEx3

System	Sensors	Measurement	Frequency	Institution
Sonic anemometer, thermometer	3	three-axis velocity components	20/s	ESRL, UConn, UHawaii
Attitude measurement system	3	roll, pitch, and yaw rates; three-axis accelerations	20/s	ESRL, UConn, Hawaii
Open path IRGA (LI-7500)	3	water vapor/CO_2	20/s	ESRL, UConn
Sleeved IRGA (LI-7500)	2	water vapor/CO_2	20/s	ESRL, LDEO
Closed path IRGA (LI-6262)	3	carbon dioxide	20/s	LDEO
Fast O_3 luminescence sensor	1	ozone	20/s	INSTAAR
DMS spectrometer	1	DMS	20/s	U. Hawaii
Pyranometer/pyrgeometer	1 each	solar and IR radiance	1/min	ESRL
Temperature, pressure, and humidity sensors	3	T, P, and RH	1/min	ESRL/UConn
Rain gauge	1	rain rate	1/min	ESRL
Sea snake surface temperature	1	sea surface temperature	1/min	ESRL
SCS	1	sea and ship met data	1/s	NOAA/*Ronald H. Brown*
Thermosalinigraph	1	sea temperature and salinity	1/s	NOAA/*Ronald H. Brown*
Air and sea CO_2 fugacity	1	fCO_2	1/15 min	NOAA/AOML
GPS and GPS compass	1	course, speed, and heading	1/s	ESRL
IR laser ceilometer	1	cloud base height	1/min	ESRL
WAMOS wave radar	1	directional wave spectra	1 scan/s	LDEO
Microwave altimeter	1	wave height	10/s	LDEO
IR laser altimeter	1	wave height	20/s	ESRL/LDEO
High-resolution camera	2	wave breaking	1/15 min	LDEO/UConn

a day with fresh water to keep the optics clean. The remaining two open path units were mounted in protective, ventilated shrouds to reduce loss of data associated with rain and sea spray [*Lauvset et al.*, 2011]. Air was pumped through one NDIR detector at 570 l min^{-1} to sample atmospheric CO_2 and H_2O fluctuations with an inlet attached near the central sonic anemometer. The shroud for this instrument was designed with a drain to allow flushing of the optics with fresh water. The second NDIR detector was supplied with atmospheric air at 200 ml min^{-1} that was first mixed in a pressure accumulator (PVC pipe) to low-pass filter real atmospheric fluctuations. The CO_2 and H_2O signals from this instrument were used as a "null" to quantify motion-induced cross talk in the measurements. This sensor was otherwise sealed and no attempt was made to clean the optics during the cruise. The cross talk will be slightly different due to differences in the instruments and motion at their respective locations. However, the null remains useful in attempts to quantify motion contamination by, e.g., looking at cross-correlation coefficients between the instruments.

Figure 4. (left) Installation of the fast sensor instrumentation on jackstaff. The central sonic anemometer was positioned 1.6 m forward of the main mast. (right) Close-up of sonic anemometers, fast humidity sensors, and mean T/RH sensors on the jackstaff of the NOAA ship *Ronald H. Brown* for SO GasEx. The PSD sonic is in the center, and the DCFS sonics are port (left in the photograph) and starboard (right in the photograph). The sleeved fast sample LI-7500 is the unit on the right with the large blue ventilation tube. The three open path units are on the left. Each sonic is mounted to its own motion-measuring system.

[19] A miniworkshop was held in July 2008 to compare instruments and motion corrections from the various systems. One of the portside NDIR analyzers did not operate properly and was not used in the analysis. The other two portside sensors and the sleeved NDIR were in good agreement during the cruise. The NOAA/ESRL/PSD system and mean of the two open paths and the sleeved ventilated LI-7500 for fast humidity are used in the investigation of COAREG given by *Fairall et al.* [2011]. The results in section 4 use the portside UConn DCFS and the two open path NDIR analyzers for fast humidity and CO_2. These two units were selected to minimize the separation between the NDIRs and the sonic anemometer. Additionally, these sensors were logged together on the UConn data acquisition system. This synchronized the NDIRs with the sonic anemometer and motion sensors as required to compute the fluxes using the direct covariance method as described by *Edson et al.* [1998] without the need to lag the time series.

4. Air-Sea Exchange of CO_2

[20] Physical controls on CO_2 transfer across the air-sea interface include vertical mixing driven by wind stress and waves, modulation of the vertical exchange by stratification and buoyancy, solubility effects driven by temperature and salinity at the sea surface and bulk seawater, and the various processes that drive ocean circulation. The general form of the air-sea CO_2 flux given by (1) can be written:

$$F_{CO_2} = k_{CO_2}\,\alpha_c\,(P_{cw} - P_{ca}) \tag{2}$$

where k_{CO_2}, P_c, and α_c are the transfer velocity, partial pressure and solubility of CO_2, respectively. A main goal of the SO GasEx program is to account for the dominant physical controls on CO_2 transfer through improved parameterization of the transfer velocity. However, another common approach to estimate surface air-sea fluxes is the so-called bulk algorithm [*Hare et al.*, 2004; *Fairall et al.*, 2011]. According to this approach, the turbulent flux of CO_2 is estimated from the mean wind speed and partial pressure differences across the air-sea interface through a transfer coefficient:

$$F_{CO_2} = C_{CO_2} S \alpha_c (P_{cw} - P_{ca}) \tag{3}$$

where C_{CO_2} is the dimensionless transfer coefficient for CO_2 (similar to the Dalton number for water vapor) and S is the mean wind speed relative to the ocean surface. Comparison of (2) and (3) implies that $k_{CO_2} = C_{CO_2} S$. Therefore, the transfer velocity is expected to vary at least linearly with wind speed [*Edson et al.*, 2008].

[21] A more exact form of the CO_2 flux between the atmosphere and ocean is given by

$$\begin{aligned} F_{CO_2} &= k_w\,(C_w - C_s) = k_a(C_s - C_a/H) \\ &= k_{CO_2}(C_w - C_a/H) \end{aligned} \tag{4}$$

where k_w, k_a, and k_{CO2} are the liquid phase, air phase, and combined gas transfer velocities, respectively; C_w, C_s, and C_a are the concentrations of CO_2 in the bulk seawater, at the oceanside interface, and in the air, respectively; and H is Henry's law constant [*McGillis et al.*, 2001a]. CO_2 is a slightly soluble gas and is primarily liquid phase controlled because of its low solubility [*Liss and Slater*, 1974; *Businger*, 1997; *McGillis et al.*, 2000]. As a result, $k_a \gg k_w \approx k_{CO2}$ and a very small gradient exists in the airside boundary layer such that

$$C_s \cong C_a/H = \alpha_{c0} P_{ca} \tag{5}$$

where P_{ca} is the partial pressure of CO_2 and α_{c0} is the solubility at the ocean surface [*McGillis et al.*, 2004]. As such, investigators have taken advantage of (5) and concentrated on the combined gas transfer velocity using the relationship

$$\begin{aligned} F_{CO_2} &= k_w(C_w - C_s) \cong k_{CO_2}(C_w - \alpha_{c0} P_{ca}) \\ &\cong k_{CO_2}(\alpha_{cw} P_{cw} - \alpha_{c0} P_{ca}) \end{aligned} \tag{6}$$

where α_{cw} and P_{cw} are the solubility and partial pressure of CO_2 in the bulk seawater. This expression reduces to (2) when the solubilities at the air-sea interface and in the bulk seawater are approximately equal as in a well-mixed oceanic surface layer.

[22] It is worth noting that the airside transfer velocity k_a can be corrected for atmospheric stability because the airside flux is driven by the most correctable airside gradient

$$c_{ca}^{1/2} = \frac{k_a}{u*} = \frac{F_{CO_2}}{(C_s - C_a/H)} \tag{7a}$$

$$c_{caN}^{1/2}(\zeta) = \frac{c_{ca}^{1/2}}{1 - \left(c_{ca}^{1/2}/\kappa\right)\psi_c} \tag{7b}$$

where c_{ca} is the airside exchange coefficient for CO_2, $u*$ is the characteristic turbulent velocity scale known as the friction velocity; N denotes the value for neutral atmospheric stability, and ψ_c represents a function that accounts for atmospheric stability based on Monin-Obukhov Similarity Theory (MOST) [e.g., *Edson and Fairall*, 1998; *Edson et al.*, 2004]. This approach has been used to estimate the flux using the gradient method for gases such as DMS by assuming that the stability function for DMS is the same as that for water vapor [*Zemmelink et al.*, 2004; *Hintsa et al.*, 2004]. However, it is extremely difficult over the ocean to implement either the gradient or bulk methods using the airside transfer velocity because $C_S \cong C_a/H$; that is, the gradient is difficult to resolve, and the surface concentration is unknown.

[23] Instead, the transfer velocity of CO_2 is more strongly affected by oceanic stratification because the flux of CO_2 is primarily waterside controlled. For example, it was shown by *McGillis et al.* [2004] that oceanic stratification modifies the CO_2 exchange in the tropics where there is large diurnal variability in the upper ocean temperature structure. However, this effect is significantly smaller in the Southern Ocean where the ocean is well mixed up to the surface [*Ho et al.*, 2011a]. This is particularly true for our measurements at moderate to high winds. Therefore, the transfer velocities from SO GasEx are expected to be close to their "neutral" values and no attempt is made to correct for stability.

4.1. Determination of Sea-Air CO_2 Flux

[24] The mixing ratio in dry air is the conservative variable required to compute the direct covariance fluxes of water vapor and CO_2

$$F_{H_2O} = \overline{\rho}_a \overline{w' r_v'} \tag{8}$$

$$F_{CO_2} = \overline{\rho}_a \overline{w' r_c'} \tag{9}$$

where w is the vertical velocity; r_v and r_c are the mixing ratios for water vapor and CO_2, respectively; and ρ_a is the density of dry air. The overbar denotes the mean of the quantity beneath it and the primes denote fluctuations in a variable about their respective means (e.g., $w' = w - \overline{w}$). The mixing ratio represents the mass of the trace gas per mass of dry air and can be related to their partial pressures; e.g., the CO_2 mixing ratio can be found from

$$r_c = \frac{m_c}{m_a}\frac{P_{ca}}{P_a} \tag{10}$$

where m_c and m_a are the molecular weights of CO_2 and dry air, respectively; P_{ca} and P_a are the partial pressures of CO_2 and dry air, respectively [*Fairall et al.*, 2000]. Note, the fugacity is also a conservative variable, $f_{ca} = \frac{m_a}{m_c} r_c = \frac{P_{ca}}{P_a}$.

4.1.1. Dilution Effects

[25] The open path LI-7500 measures the mass concentrations in moist air rather than mixing ratio. Therefore, the fast CO_2 concentration signals obtained from these instruments used in our study require a number of corrections to obtain the CO_2 flux. The so-called dilution correction [*Webb et al.*, 1980] accounts for the nonconservative nature of the mass concentration variable [*Fairall et al.*, 2000; *Edson et al.*, 2008]. The mass concentrations can be related to the specific humidity, q, and specific CO_2 concentration, s_{CO_2}, as

$$q = \frac{m_v}{M}\frac{P_v}{P} = \frac{m_v}{M}\mathrm{X}_v = \frac{R_g T}{MP}\chi_v \tag{11}$$

$$s_{CO_2} = \frac{m_c}{M}\frac{P_{ca}}{P} = \frac{m_c}{M}\mathrm{X}_c = \frac{R_g T}{MP}\chi_c \tag{12}$$

where m_v is the molecular weight of water vapor; M is the molecular weight of moist air; P is the (total) air pressure; X_v and X_c are the mass concentrations (often given as mole fraction) of water vapor and CO_2 in moist air, respectively; $R_g = 8.314\ \mathrm{Pa\ m^3\ mole^{-1}\ K^{-1}}$ is the ideal gas constant; and χ_v and χ_c are the mass densities of water vapor and CO_2, respectively [*Fairall et al.*, 2000].

[26] Some investigators attempt to estimate the mixing ratio directly from NDIRs by drying the sample and bringing it to equilibration with temperature prior to measurement

$$r_c = \frac{m_c}{m_a}\frac{P_{ca}}{P_a} = \frac{m_c}{m_a}\mathrm{X}_c^{dry} \tag{13}$$

where X_c^{dry} is the mass of CO_2 per mass of air that has been dried and thermalized. Samples that have been dried (e.g., with a Nafion tube) would have to be corrected for temperature fluctuations only [e.g., *Miller et al.*, 2009, 2010]. The approach used here is to "dry" the samples numerically by applying an additional dilution correction to estimate the mixing ratio

$$r_v = \frac{q}{(1-q)} \tag{14}$$

$$r_c = \frac{s_{CO_2}}{(1-q)} = \frac{m_c}{M}\frac{\mathrm{X}_c}{(1-q)} = \frac{R_g T}{MP}\frac{\chi_c}{(1-q)} \cong \frac{R_g T}{m_a P}\chi_c\left(1 + \frac{m_a}{m_v} r_v\right) \tag{15}$$

[27] The mass concentrations (or mole fractions) X_v and X_c are typically output by closed path sensors such as the LI-6262 using internally measured pressure and temperature. The mass densities χ_v and χ_c are the "raw" values that we collect from the open path LI-7500 used in this experiment.

[28] The temperature and humidity measurements of the ambient air are computed using a combination of fast and slow response sensors for the fluctuations and means, respectively. Vaisala PTU200 sensors were used for the mean pressure, temperature and humidity. The sonic thermometer and LI-7500 were used to provide the fast temperature and humidity measurements. For example, the PTU200s were used to compute the mean temperature and specific humidity. The LI-7500 and sonic temperature were then used to compute the fluctuations about these means.

[29] Additionally, *Miller et al.* [2010] have shown that the hydrostatic pressure fluctuations can add significant motion-induced signal to the CO_2 time series, which can be removed with a fast response pressure sensor. However, the PTU200 pressure sensor has a 2 s response time and is averaged over 1 s, so it is not optimal for this correction. Instead, the heave calculated from the DCFS is used to compute the fluctuating hydrostatic pressure from $-\rho g \Delta z$, where Δz is the fluctuation in heave. The fluctuating component was added to the mean pressure to generate the time series used in this analysis. This signal is in good agreement with the pressure sensor after lagging the latter by approximately 3 s. However, the pressure computed by the heave has much better resolution and does not suffer from dynamic pressure contamination. These measurements are used with (14) and (15) to provide time series estimates of the mixing ratios required to compute the fluxes.

[30] In principle, fluxes of CO_2 could be computed using (9) by correlating time series estimates of mixing ratio from (15) with motion corrected vertical velocity measurements. *Fairall et al.* [2000] expanded (15) into its mean and fluctuating components and showed that this is equivalent to

$$\overline{\rho}_a \overline{w' r_c'} = \overline{w' \chi_c'} + \left[\frac{m_a}{m_v}\overline{w' r_v'} + \left(1 + \frac{m_a \overline{r_v}}{m_v}\right)\frac{\overline{w' T'}}{\overline{T}}\right]\overline{\chi}_c \tag{16}$$

which shows the required correction to the flux due to the water vapor and temperature fluxes. However, NDIRs are subject to additional cross talk with water vapor associated with pressure broadening and optical surface contamination.

4.1.2. Humidity Cross Talk and Pressure Broadening

[31] The internal LI-7500 algorithm for CO_2 is expected to account for pressure broadening (LI-7500 CO_2/H_2O Analyzer Instruction Manual, pp. 2–7, 8, LiCor Inc., Lincoln,

NB). The combination of this correction with the dilution correction described above appears sufficient for closed path sensors such as the LI-6262 using short sampling tubes after correction for the motion induced noise [*McGillis et al.*, 2001a]. However, recent field studies with LI-7500 open path instruments have revealed inconsistent performance for CO_2 flux calculations [*Kondo and Tsukamoto*, 2007], and unexpected water vapor cross talk due to optical surface contamination appears to be the culprit [*Kohsiek*, 2000]. Similar results were seen in SO GasEx where the open path LI-7500 units had much higher water vapor cross talk than was experienced with closed path units in the two previous GasEx field programs.

[32] The shrouded LI-7500 were developed and deployed in an attempt to reduce the optical surface contamination. Unfortunately, the open path and shrouded NDIR used to compute the fluxes exhibited similar levels of water vapor cross talk. The water vapor cross talk is much lower for the shrouded "null" sensor, partly because water vapor fluctuations that drive much of the cross talk (see below) are low-pass filtered by the mixing volume. Postcruise tests indicate that a problem with the water vapor correction provided by LiCor is not the sole cause of the cross talk observed in the field. Specifically, laboratory tests show that the LiCor water vapor correction is not exact, but the error is on the order of 15% of the dilution correction for the unit tested. That is significantly smaller than the water vapor cross talk observed in SO GasEx. Additionally, the optics of the open path and shrouded NDIR were freshwater flushed daily so the accumulation of salt from sea spray is an unlikely cause of the contamination.

[33] Instead, it is believed that the optics were contaminated by small particles that includes soot emanating from the diesel engines and organic deposits from small sea spray particles that pass through the shroud intake. This is based on observations from prior cruises where a sooty film was visible on the optics of sensors that were not regularly cleaned. Although this needs to be evaluated more thoroughly, it is hypothesized that the organic film builds up quickly between flushings and/or are not completely removed during the flushing process. This did not impact the null sensor because the air source was passed through the mixing volume, and then sucked down a very small tube with low flow. Therefore, it is hypothesized that the null remains less contaminated because the small particles are much more efficiently removed before reaching the sensor.

[34] As a result, all the NDIRs used to sample CO_2 fluctuations in the ambient air require correction to remove the water vapor cross talk. *Prytherch et al.* [2010a] have developed a "dynamic" method to compute a cross talk correction from the signals assuming that the correlation between water vapor and airside CO_2 should obey MOST. This approach has been dubbed the "PKT method" as it was first suggested by Peter K. Taylor from the University of Southampton. In the remainder of this section, a modification to the PKT method is developed and applied to the SO GasEx data.

[35] Suppose there is some form of crosstalk of water vapor with the LI-7500 CO_2 signal so that

$$r'_{cm} = r'_c + \mu r'_v \tag{17}$$

where r'_c is *true* fluctuation of CO_2 mixing ratio, r'_{cm} is the measured value from the LI-7500 after dilution correction, r'_v is the fluctuation in the water vapor mixing ratio and μ the crosstalk coefficient. Here, the mixing ratio is used for convenience; similar results are obtained if the relative humidity has also been used as per the PKT method. This affects the flux directly by

$$\overline{w'r'_c} = \overline{w'r'_{cm}} - \mu\overline{w'r'_v} \tag{18}$$

[36] The crosstalk coefficient can be found by multiplying both sides of (17) by r_v', taking the average, and solving for μ

$$\mu = \frac{\overline{r'_v r'_{cm}} - \overline{r'_v r'_c}}{\overline{r'_v r'_v}} \tag{19}$$

The second term in the numerator of (19) is the real cross correlation of water vapor and CO_2 associated with surface driven turbulent exchange. The spectral representation of (18) is

$$C_{wr_c}(\omega) = C_{wr_{cm}}(\omega) - \mu(\omega)C_{wr_v}(\omega) \tag{20}$$

where the spectral correction coefficient is

$$\mu(\omega) = \frac{C_{r_v r_{cm}}(\omega)}{S_{r_v r_v}(\omega)} - \frac{C_{r_v r_c}(\omega)}{S_{r_v r_v}(\omega)} \tag{21}$$

where C_{xy} is the cospectrum of x and y, S_{xx} is the variance spectrum of x, and ω is the frequency.

[37] Implementation of the cross-correlation method to correct for humidity crosstalk via (18) or (20) requires an estimate of the actual cross correlation of water vapor in (19) or (21). Various means to estimate this term are provided in Appendix A. However, the magnitude and spectral form of the correction can be readily shown by simplifying (21) to read

$$\mu(\omega) = \left(1 - \frac{C_{r_v r_c}(\omega)}{C_{r_v r_{vm}}(\omega)}\right)\frac{C_{r_v r_{cm}}(\omega)}{S_{r_v r_v}(\omega)} \cong \Gamma\frac{C_{r_v r_{cm}}(\omega)}{S_{r_v r_v}(\omega)} \tag{22}$$

Good agreement is obtained between the fluxes computed using the PKT approach and integration of (20) using $\Gamma = 0.88$. This value suggests that the actual cross correlation is approximately 12% of the measured cross correlation.

[38] The PKT method is an iterative approach that reduces the observed dependence of CO_2 on the relative humidity until the expected dependence is reached. The expected dependence is determined from the CO_2 and moisture fluxes calculated from the time series [*Prytherch et al.*, 2010a]. Therefore, although integration of the cospectrum computed from the adjusted time series will provide the same value of the flux, it cannot be expected to give the correct cospectral shape. In fact, it appears to overcorrect the low-frequency components while under correcting the higher-frequency components if similarity between the moisture and CO_2 cospectra is assumed.

[39] Therefore, a principle advantage of the approach presented here is that is allows an examination of the spectral response over a wider range of frequencies to various sources of noise. An example of the cospectral terms in

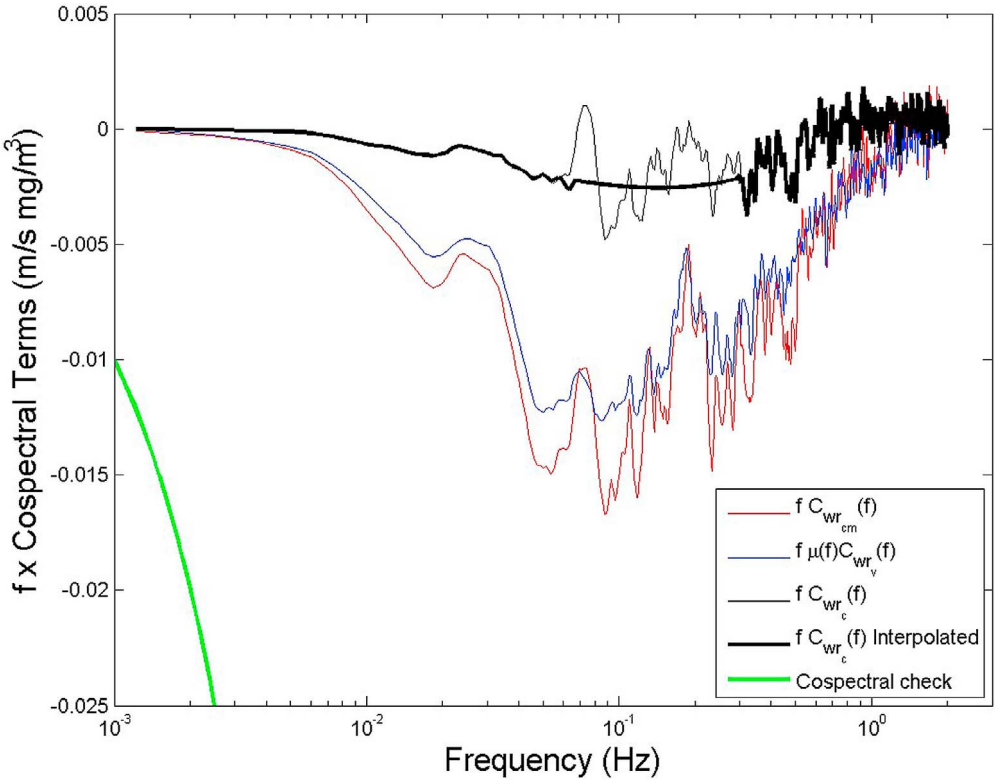

Figure 5. The cospectral terms given in (20) after correction for the heave-induced hydrostatic pressure fluctuations in (15). The red line is the vertical velocity–CO_2 cospectrum averaged over wind speed between 10 and 10.5 m s^{-1}. The blue line is the CO_2-H_2O cospectrum multiplied by the correlation coefficient given by (22). The thin black line is their difference and represents the cospectrum corrected for humidity cross talk and remaining motion contamination. The thick black line represents a third-order fit to the data on either side of 0.06 and 0.3 Hz, which reduces the uncertainty due to the remaining contamination of the sensor. The green line represents the cospectral check criterion described in section 4.3.

(20) is shown in Figure 5, where the cospectra are averaged over wind speeds between 10 and 10.5 m s^{-1} and μ has been determined from (22) using $\Gamma = 0.88$. The cross talk is a significant fraction of the measured $C_{wr_{cm}}(f)$ cospectra over all frequencies. The corrected flux is approximately an order of magnitude smaller than the measured flux, which is in agreement with the result reported by *Prytherch et al.* [2010a].

[40] The spectral approach also allows the identification of motion-induced noise in our flux estimates. This can be easily seen through comparison of Figures 5 and 6. The heave-induced pressure perturbations are used in (15) to compute the cospectra shown in Figure 5, while only the mean pressure has been used in Figure 6. The removal of the hydrostatically induced pressure changes significantly alters the behavior of the cospectra at wave frequencies. Therefore, it appears that a significant fraction of this motion-induced noise is simply due to hydrostatic perturbations in pressure as suggested by *Miller et al.* [2010].

[41] Some noise remains due to mechanical responses to ship motion that impacts both CO_2 and H_2O measurements. For example, *McGillis et al.* [2001a] hypothesized that motion-induced noise is driven by gyroscopic effects on the chopper wheel used in the LI-6262 and LI-7500, while *Miller et al.* [2010] suggested that any remaining motion-induced noise is due to flexing of the source filament. However, it appears that the spectral approach removes most of the remaining noise in our flux estimates. This is because the motion-induced noise is highly correlated between the CO_2 and H_2O signals from the same instrument. In fact, this would include most of the signal associated with heave-induced hydrostatic fluctuations as shown in Figure 6. Therefore, the cross-talk method would be effective at reducing the noise even if the mean pressure is used in the dilution correction. However, it is clearly more satisfactory to include the pressure perturbations in the dilution correction prior to computation of the cospectra. The cross-talk method is then used to remove the humidity cross talk and the remaining motion-induced noise as in Figure 5.

[42] This analysis shows that the motion induced noise in the measured CO_2 signal tends to be positively correlated with the vertical velocity, which reduces the magnitude of the downward flux between 0.06 and 0.3 Hz. The thick black line in Figure 5 represents a third-order fit to the data on either side of this range. The cospectra are integrated under this curve to further reduce some of the uncertainty in the spectrally computed fluxes. Therefore, the cospectra are corrected using $\Gamma = 0.88$ with the procedure outlined above to compute the fluxes used in section 4.3. It should be noted that both the constant Γ and PKT corrected fluxes give very

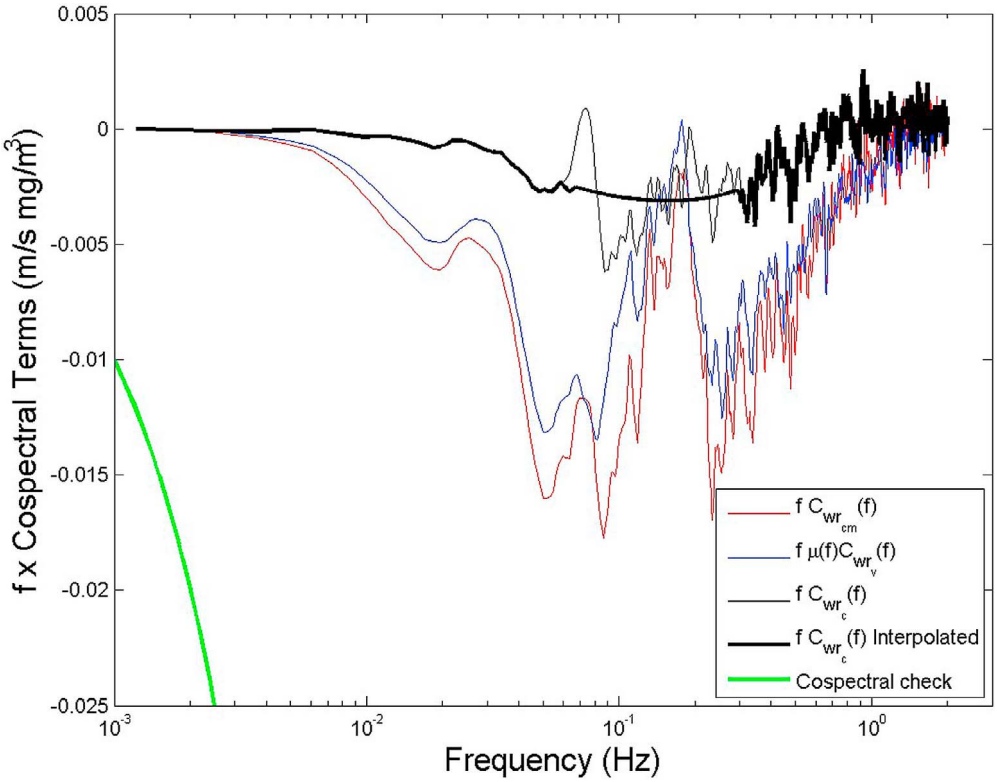

Figure 6. The cospectral terms given in (20) after inclusion for the mean pressure only in (15). The red line and blue lines are as in Figure 5. The thin black line is their difference and represents the cospectrum corrected for humidity cross talk and motion contamination, which includes the hydrostatic pressure perturbations. The thick black line represents a third-order fit to the data on either side of 0.06 and 0.3 Hz, which reduces the uncertainty due to the remaining contamination of the sensor.

similar result since the coefficient in (22) is tuned to agree with the PKT values on average. However, the spectrally corrected fluxes are used in the following analysis because they give slightly smaller standard error in the averaged transfer velocities than PKT. It is hypothesized that the smaller error is mainly due to more effective removal of the remaining motion-induced noise with the spectral correction. An alternative to the constant Γ approach that relies on MOST is described in Appendix A.

4.2. Determination of Sea-Air CO_2 Concentration Differences

[43] The concentration of carbon dioxide in the near surface ocean water is determined by measuring the concentration of CO_2 in gas that is in contact with the water using an equilibrator. Surface water was pumped from a bow inlet at nominally 5 m depth to an equilibrator located in one of the aft laboratories. The equilibrator has a spray nozzle in the headspace and a pool of seawater this is continuously overflowing through an air trap drain. The principle of operation of the headspace spray equilibrator is that of *Weiss* [1970]. As the water flows through the equilibrator, the partial pressure, P_c, or fugacity, f_c, in the headspace equilibrates with the water. The difference between the fugacity in the headspace and in the water is determined by a known relationship between fugacity and mass concentration (mole fraction) that depends on temperature, salinity, and pressure. For example, the fugacity of the seawater is determined from the mole fraction using the empirical relationship derived by *Takahashi et al.* [1993]:

$$f_{cw}(T_w) = \mathrm{X}_{cw}(T_{eq})(P_{eq} - P_v)\exp\lfloor\lfloor B(CO_2, T_w) + 2\delta(CO_2, T_w)\rfloor P_{eq}/R\ T_w\rfloor \quad (23)$$

where T_w is the inlet temperature; P_{eq} and T_{eq} are the pressure and temperature in the equilibrator, respectively; and P_v is the partial pressure of water vapor. The parameters R, $B(CO_2, T_w)$ and $\delta(CO_2, T_w)$ are the virial coefficients for CO_2 [*Weiss*, 1974]. In practice, the inlet temperature is also adjusted to the skin temperature using a bulk formula [e.g., *Fairall et al.*, 1996a] before inclusion in (23) to account for the thermal gradients in the gas diffusive microlayer [*McGillis and Wanninkhof*, 2006].

[44] The mass concentrations of CO_2 in the atmosphere and the water from the equilibrator are computed from their respective mixing ratios. The mixing ratios of dried equilibrated air are calculated by fitting a second-order polynomial through the hourly averaged response of the detector versus mixing ratios of the standards. The mixing ratios are converted to mole fraction using $\mathrm{X}_c^{Dry} = r_c m_a/m_c$ and the value of X_{ca} in the equilibrator headspace and X_{cw} used in (23) are calculated by assuming 100% water vapor content. Conversion between fugacity and partial pressure can be

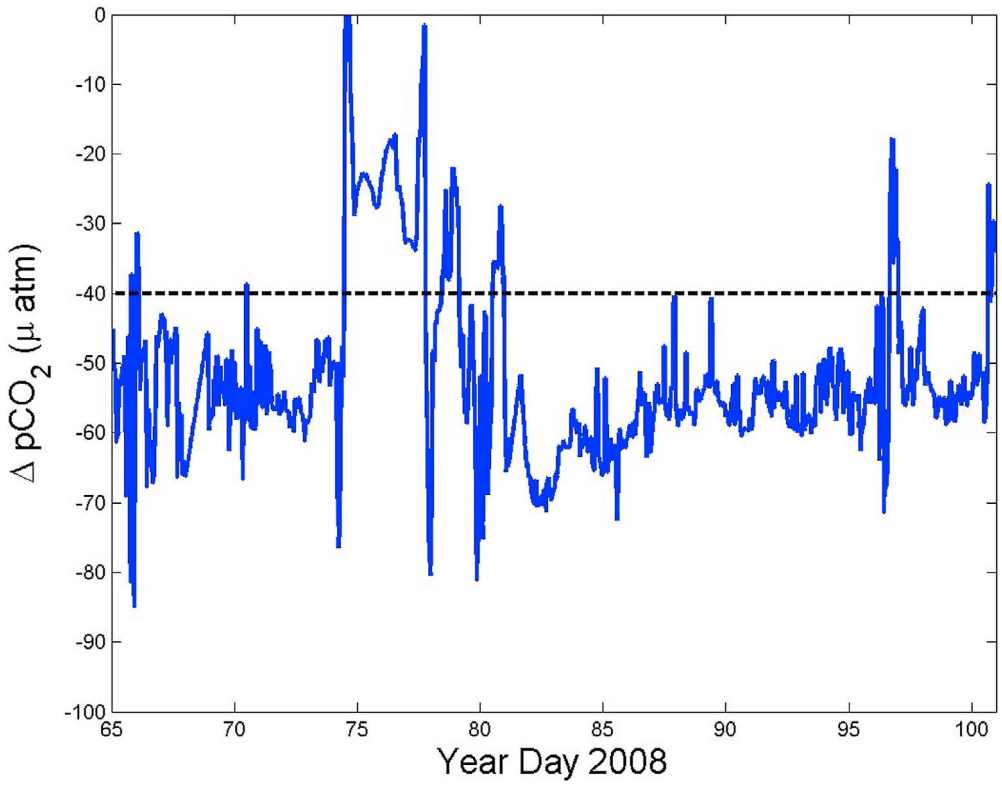

Figure 7. Time series of the atmosphere-ocean partial pressure difference measured during SO GasEx. The dotted line represents the upper limit of the negative values used in our analysis. The data are courtesy of Rik Wanninkhof, NOAA AOML.

carried out using a set of standard procedures [*U.S. Department of Energy*, 1994; *Dickson et al.*, 2007]. The time series of ΔP_c (or ΔpCO_2) measured during SO GasEx are shown in Figure 7 (courtesy of Rik Wanninkhof, NOAA AOML).

4.3. Wind Speed–Dependent Transfer Velocity

[45] The transfer velocity for CO_2 is computed from our direct covariance CO_2 fluxes divided by the sea-air CO_2 difference

$$k_{CO_2} = \frac{F_{CO_2}}{\alpha_{cw}(P_{cw} - P_{ca})} = \frac{F_{CO_2}}{\alpha_{cw}\Delta P_c} \tag{24}$$

where measurement of $\alpha_{cw}\Delta P_c$ is described in 4.0 and 4.2, and the flux is computed from the procedure described in 4.1. The transfer velocities are adjusted to a Schmidt number of 660 using

$$K_{660} = k_{CO_2}\left(\frac{Sc_{CO_2}}{660}\right)^{1/2} \tag{25}$$

where Sc_{CO_2} is the CO_2 Schmidt number under ambient conditions. The multiplier increases the measured values of the transfer velocity k_{CO_2} in calculating K_{660} because the diffusivity for CO_2 in the cold water of the Southern Ocean is low, making the Schmidt number is larger than 660.

[46] As explained above, due to the nature of CO_2 as a waterside controlled gas, no attempt is made to correct the transfer velocity for stability. However, the wind speeds used in the analysis are adjusted to a reference height of 10 m and neutral conditions using MOST. Correction of the wind speed to neutral conditions attempts to account for the effect of stability on atmospheric forcing that drives waves and subsurface turbulence, which then controls the waterside exchange of CO_2. Therefore, the measured transfer velocities are plotted versus the neutral value of the wind speed adjusted to 10 m, U_{10N}, to account for atmospheric stability [e.g., *Fairall et al.*, 2003].

[47] Figure 8 (top) shows the fluxes computed from 15 min time series. The data shown in this plot has passed the following criteria: (1) $\Delta P_c = \Delta pCO_2 < -40$ μatm, (2) $-90° <$ relative wind $< 50°$, (3) LiCor AGC $< 84\%$, (4) RH $< 95\%$, (5) bulk estimate of the latent heat flux >25 Wm^{-2}, and (6) absolute value of individual cospectral estimates $|C_{wr_c}(f)| <$ 10 mg m^{-2}.

[48] The first criterion is required to provide sufficient CO_2 signal-to-noise for direct covariance measurements [*Ho et al.*, 2011a]. The second criterion provides good exposure for the sonic anemometer/LI-7500 pair positioned on the port side of the jackstaff above the bow. The next three criteria act to remove data that are overly contaminated by dirty or wet optics. The AGC (automatic gain control) is a diagnostic parameter output by the LI-7500 indicating the cleanliness of the optics. The AGC for the cleanest optics are 50%–60% and go to 98% in rain and fog. The combination of the RH and latent heat flux criteria significantly reduces the scatter due to fog and condensation on the optics; that is, high RH and small (sometimes negative) bulk estimates of the latent heat flux are nearly always accompanied by fog.

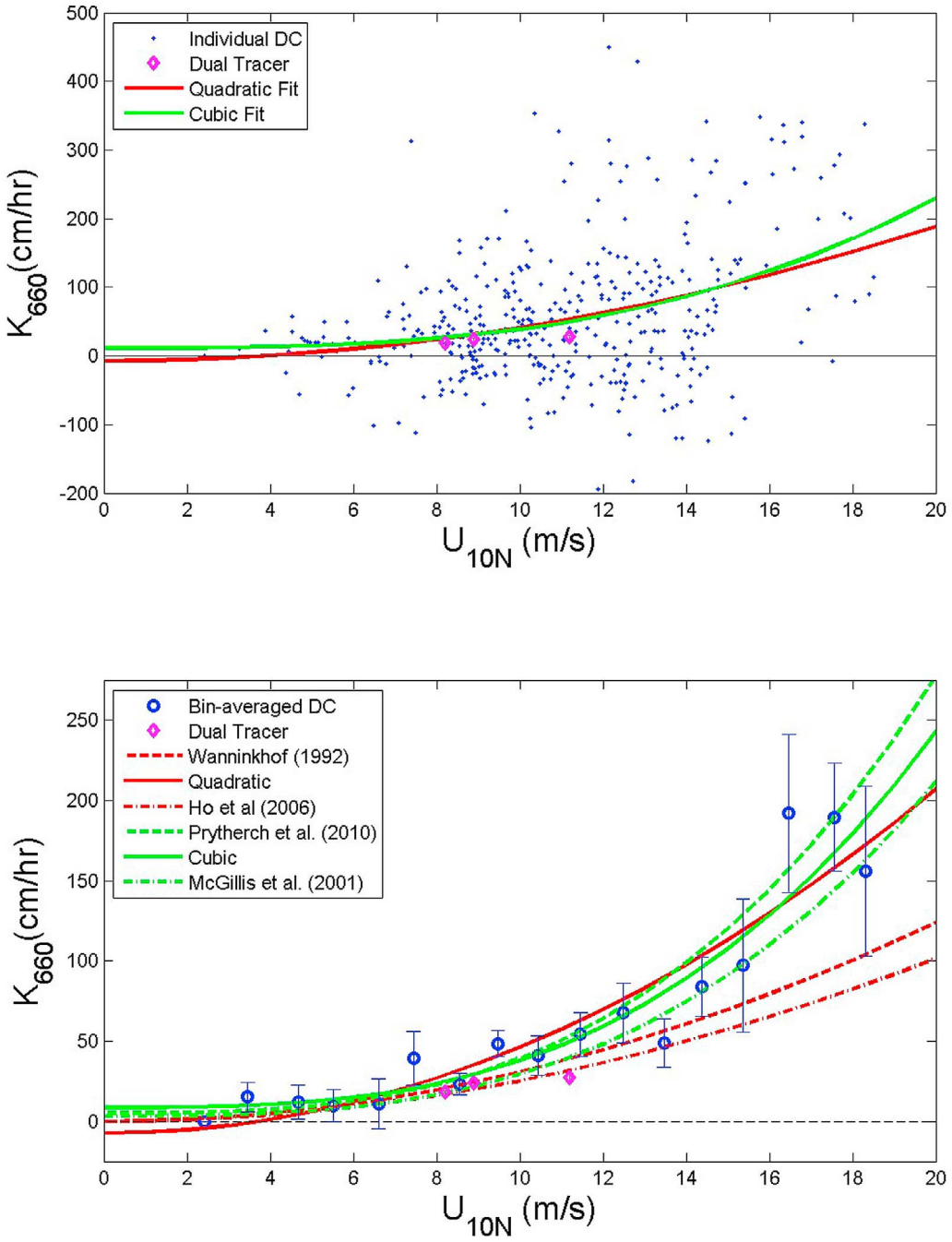

Figure 8. Measured values of the transfer velocity from the SO GasEx program. (top) Individual data points and (bottom) bin-averaged values. The averages are computed from 1 m s^{-1} wind speed bins. The magenta diamonds are the transfer velocities computed from the dual tracer technique reported by *Ho et al.* [2011b] after adjustment to a Schmidt number of 660. The error bars represent the standard error about the mean. The solid red and green lines represent quadratic and cubic fits, respectively, to the individual data (Figure 8, top) and bin-averaged data (Figure 8, bottom). The dashed red line represents the relationship given by *Wanninkhof* [1992], $K_{660} = 0.31U_{10N}^2$; the dash-dotted red line is from *Ho et al.* [2006], $K_{660} = 0.254U_{10N}^2$; the dashed green line is from *Prytherch et al.* [2010b], $K_{660} = 0.034U_{10N}^3 + 5.3$; and the dash-dotted green line is the cubic relationship from *McGillis et al.* [2001a], $K_{660} = 0.026U_{10N}^3 + 3.3$.

The last criterion is graphically shown by the green line in Figure 5 and effectively removes spectra that are poorly behaved at low frequencies. Most of contaminated data are removed by the first 5 criteria and this last criterion removes the few remaining outliers.

[49] Figure 8 (bottom) shows the bin-averaged results computed where the averages and standard errors are computed from the data in 1 m s^{-1} bins. Also shown are the quadratic wind speed parameterization reported by *Wanninkhof* [1992] and *Ho et al.* [2006], and the cubic

relationship reported by *McGillis et al.* [2001a] and *Prytherch et al.* [2010b]. It should be noted that these particular quadratic relationships go to zero at light winds, while the cubic relationships allow for a small positive offset as the mean wind speed goes to zero. One possible mechanism for the nonzero transfer velocity is variability in the wind associated with gustiness that continues to drive heat, mass and momentum exchange as the average wind vector goes to zero [*Fairall et al.*, 1996b; *McGillis et al.*, 2004]. A similar explanation for nonzero transfer velocities based on waterside convection is given by *MacIntyre et al.* [2001] and *Rutgersson et al.* [2011]. Yet another factor that could lead to a nonzero intercept is the chemical enhancement of CO_2 as described by *Wanninkhof and Knox* [1996].

[50] A quadratic dependence of the transfer velocity on wind speed based primarily on dual tracer experiments is most frequently encountered in the literature. However, in recent years, bubble-mediated enhancement of the transfer velocity, which approximately exhibits a cubic relationship with wind speed, has emerged as a key issue for flux parameterization in high-wind regions [e.g., *Woolf*, 1997; *Wanninkhof and McGillis*, 1999]. Therefore, a major question to be addressed in SO GasEx is whether the transfer velocities obey a quadratic or cubic relationship with wind speed. Unfortunately, it is difficult to unambiguously resolve this question due to the uncertainty in our transfer velocity estimates, particularly at wind speed greater than 12 m s^{-1}. This uncertainty is largely driven by the low signal-to-noise ratios in individual flux estimates resulting from the humidity cross talk described in section 4.1.2. However, results from the GasEx experiments conducted in the North Atlantic in 1998 [*McGillis et al.*, 2001a] and the equatorial Pacific [*McGillis et al.*, 2004] can be combined with the SO GasEx data to reduce some of the uncertainty. The transfer velocities taken during the previous GasEx experiments, which relied on closed path systems with short sampling tubes, have significantly less scatter than SO GasEx in Figure 9.

[51] The nature of the wind speed dependence is investigated using the individual data and several approaches to bin average the data. For example, all of the individual data from GasEx 98 (1449 data point), GasEx 01 (649 data points) and SO GasEx (414 data points) are combined before bin averaging to generate the data shown in Figure 10. The top plot uses equally spaced 1 m s^{-1} wind speed bins to average the transfer velocities. As such, the number of points within each bin is expected to vary. The bottom plot divides the data into 16 bins with an equally distributed number of observations in each bin. This procedure is repeated by first producing equally spaced and equally distributed bin-averaged estimates for each field experiment (e.g., the equally space data shown in Figure 9) and then combining all of the data to produce equally spaced and equally distributed bin-averaged estimates for analysis (Figure 10). The bin-averaged transfer velocities are then fit to the average of the wind speed ($\overline{U_{10N}}$), the average of the wind speed squared ($\overline{U_{10N}^2}$), or the average of the wind speed cubed ($\overline{U_{10N}^3}$) in each bin. The quadratic and cubic fits to the data are shown by the red and green lines, respectively, in Figures 8–10 for six of the eight fits summarized in Table 2.

[52] Although the linear fit has a reasonably high R^2 value, it performs worse than either quadratic or cubic model. Similar "goodness of fit" based on the R^2 values are found between two quadratic and cubic formulations. However, the coefficient for the cubic parameterization has less uncertainty than the quadratic (i.e., the standard deviation divided by the mean is 1.8% versus 7.4%), and has a higher average R^2 values than quadratic. The y intercept of the quadratic relationship also has the undesirable characteristic of being negative. This gives unrealistic values of the transfer velocity that go below zero at low wind speeds.

[53] The data below 10 m s^{-1} fit either the quadratic or cubic parameterizations equally well. However, inclusion of the data for wind speeds above 12 m s^{-1} indicate that the cubic relationships from either *McGillis et al.* [2001a] or *Prytherch et al.* [2010b] are a better fit. The good agreement with *McGillis et al.* [2001a] is not surprising since that formulation is based on the GasEx98 data set. Comparison of the bin averages in Figures 9 (bottom) and 10 (top) show that the coefficients for the equally spaced wind speed bins is largely driven by the high-wind SO GasEx data. However, it is reassuring that the equally spaced and equally distributed data (which are more equally distributed between the GasEx 98 and SO GasEx data at moderate to high winds) give very similar coefficients. Therefore, the average of the coefficients denoted by * provide a cubic relationship given by

$$k_{CO_2} = \left(0.029\, U_{10N}^3 + 5.4\right)\left(\frac{660}{Sc_{CO_2}}\right)^{1/2} \tag{26}$$

where the Schmidt number correction required to compute the fluxes under ambient conditions is included. Equation (26) is in good agreement with the relationship given by *Prytherch et al.* [2010b], which is based on a completely different data set taken aboard the weathership Polarfront in the North Sea. The good agreement between the GasEx 98, *Prytherch et al.* [2010b] and SO GasEx studies indicates that high-latitude transfer velocities in the North Atlantic agree with those from the Southern Ocean.

5. Discussion

[54] As stated above, the previous quadratic relationships fit both the direct covariance and dual tracer data reasonable well for wind speeds less than 10 m s^{-1} (e.g., see the discussion by *Ho et al.* [2011b]). The same finding holds for SO GasEx where the dual tracer estimates below 10 m s^{-1} fall within the standard error of the SO GasEx data (Figure 8). Historically, this is where most of the dual tracer estimates lie due to the integration time required to estimate the transfer velocity combined with difficulty in finding suitable regions with sustained high winds for extended periods. However, the direct covariance measurements from the GasEx programs argue for a larger value coefficient of the transfer velocities at high wind speeds compared to other commonly used parameterizations such as *Wanninkhof* [1992], *Nightingale et al.* [2000], and *Ho et al.* [2006], of which the latter two are primarily based on dual tracer estimates. Since the measured drag coefficients were similar to the nominal ocean values used in COARE [*Fairall et al.*, 2011], the enhanced CO2 transfer at high winds is not caused by unusually large drag coefficients or u_* values.

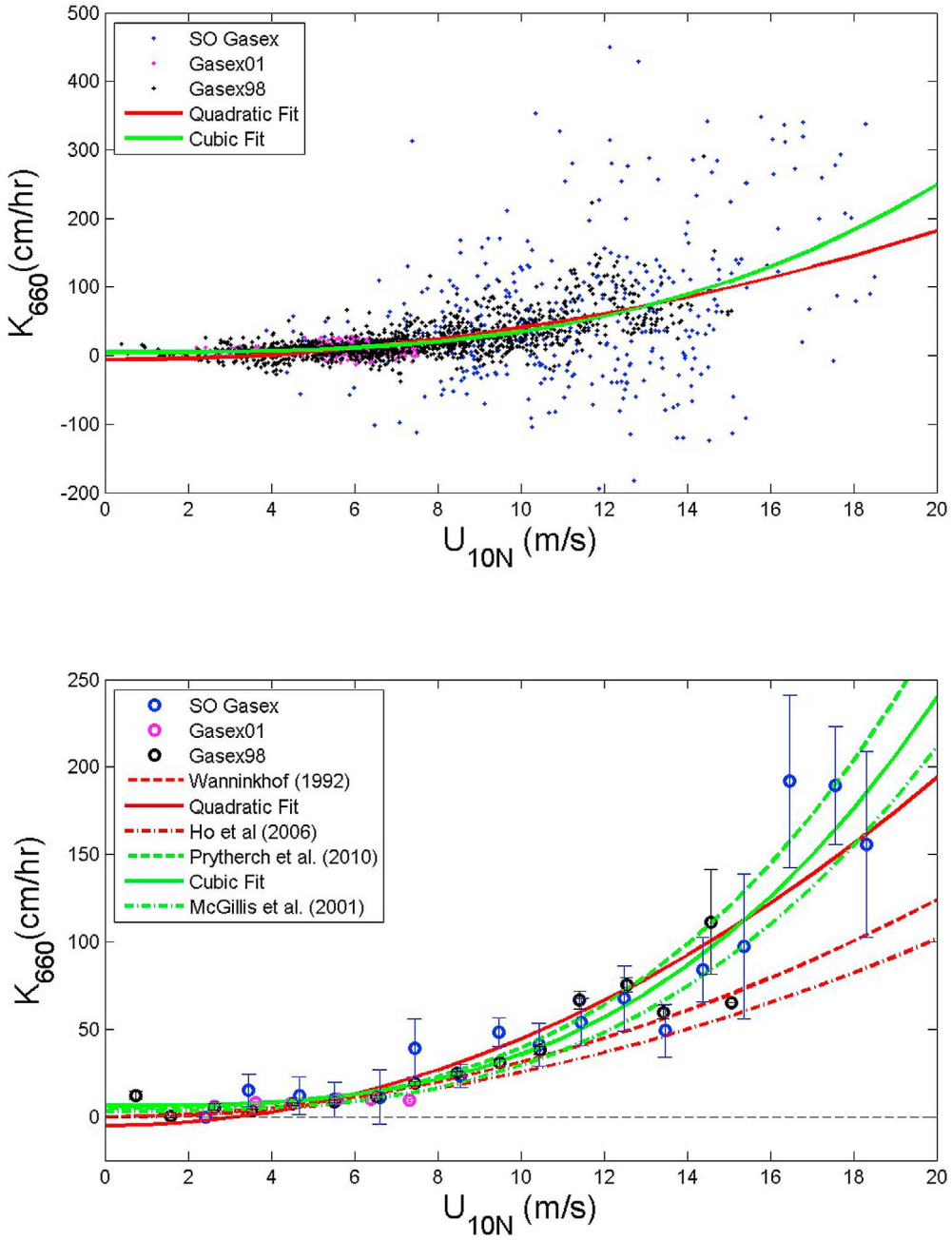

Figure 9. Measured values of the transfer velocity from the GasEx 98, GasEx 01, and SO GasEx field programs. The data are as presented in Figure 8. The quadratic and cubic fits are (top) to all of the individual data and (bottom) to all of the bin-averaged values from the three field programs.

[55] It can be argued that the difference between these estimates is due to processes that govern air-sea exchange differently for individual gases at high winds. For example, it has been hypothesized that waterside diffusion and turbulence are largely responsible for turbulence exchange at lower wind speeds [e.g., *Woolf*, 1997], while bubble mediated transfer becomes increasing important at high winds. Therefore, differences between the exchange of CO_2 and the gases used in the dual-tracer method (i.e., $^3He/SF_6$) at high winds due to bubble mediated exchange are a possible cause for the differences. Observations are showing evidence for this with other gases. For example, there is increasing evidence that the transfer velocity for DMS at high wind speeds is less that of CO_2 [*Blomquist et al.*, 2010; *Yang et al.*, 2011]. It has been suggested that this is due to differences in their relative solubilities as the void fraction in the near surface ocean increases due to breaking waves [e.g., *Vlahos and Monahan*, 2009].

[56] The COAREG [see *Fairall et al.*, 2000, 2011] algorithm attempts to parameterize these processes in the transfer velocity using two components: one that accounts for exchange due to diffusion and turbulence and another that accounts for bubble-mediated exchange. The black line in Figure 10 represents the COAREG algorithm for CO_2,

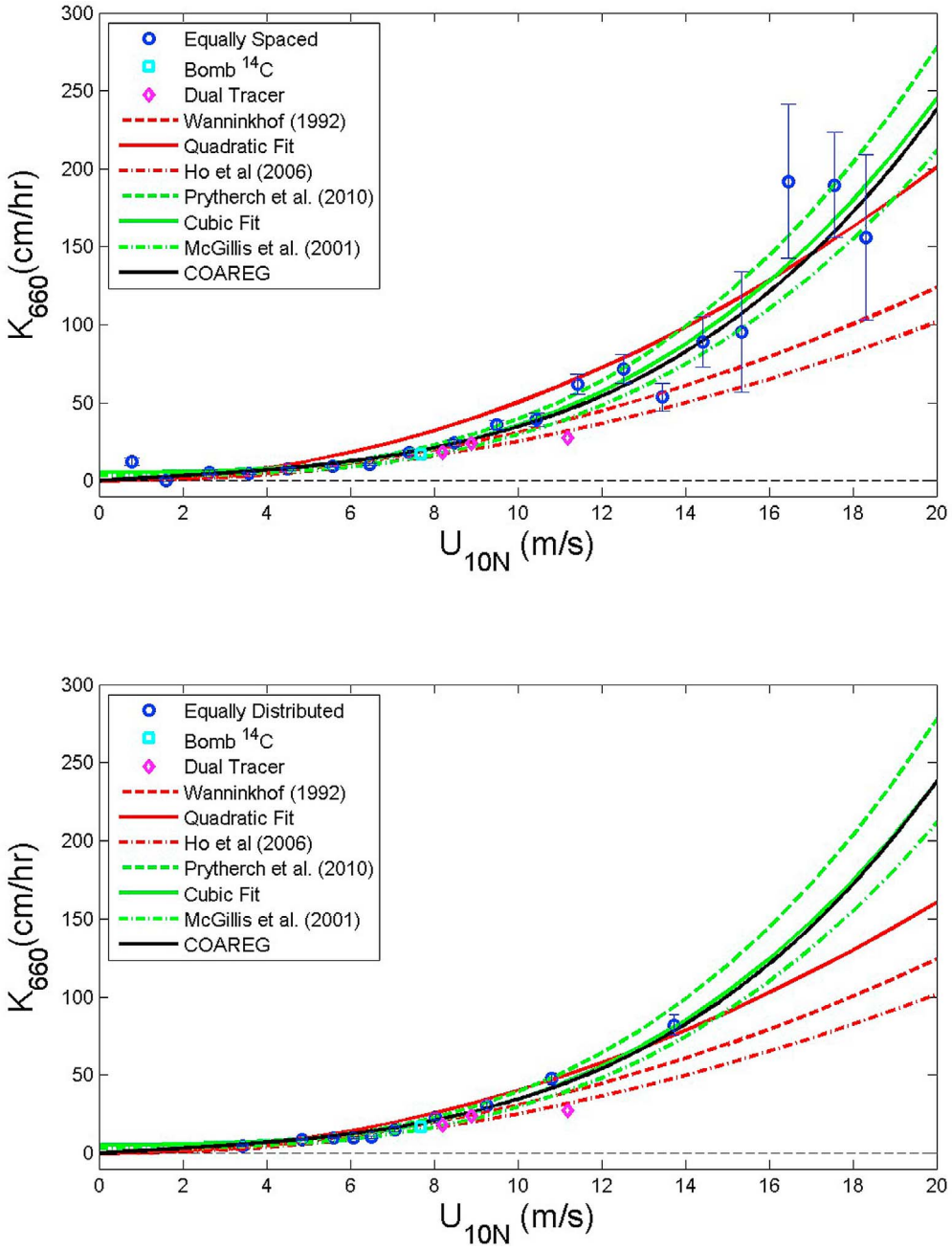

Figure 10. Bin-averaged data computed after combination of all transfer velocity measurements collected during the GASEX 98, GASEX 01, and SO GasEx field programs in a single data file. (top) The bin averages for equally spaced wind speed bins. (bottom) The bin averages for an equally distributed number of points within 16 bins. The red and green lines represent quadratic and cubic fits to the bin-averaged data. The black line represents the COAREG algorithm for CO_2, which has been tuned to fit the equally distributed averages with turbulent/molecular coefficient A = 1.5 and bubble-mediated coefficient B = 2.6. The parameterizations are as given in Figures 8 and 9. The dual tracer measurements and the transfer velocity estimate based on the global excess ^{14}C data as reported by *Naegler et al.* [2006] are also shown.

which has been tuned to fit equation (26) using a turbulent/molecular coefficient A = 1.5 and bubble-mediated coefficient B = 2.6. The fluxes from the tuned COAREG algorithm can be averaged over the same time intervals used to compute the transfer velocities from the dual tracer estimates. These fluxes can be divided by the average ΔP_c to compute the average transfer velocity over these periods. The continuous nature of the COAREG fluxes allows for a more direct comparison with dual tracer estimates that includes the naturally occurring variability.

[57] The results from this comparison are summarized in Table 3, where the transfer velocity that accounts for

Table 2. The Coefficients Obtained From Least Square Fits to the Data[a]

	$K_{660} = mU^N + b$			$K_{660} = mU^N$	
	m	b	R^2	m	R^2
Linear: N = 1					
IP SOG	10.377	−57.8	0.100	5.474	0.078
ES SOG	10.884	−49.9	0.789	6.965	0.687
ED SOG	10.385	−58.1	0.725	5.459	0.562
ES IFC*	8.944	−34.0	0.767	5.925	0.679
ED IFC*	8.663	−40.6	0.811	4.307	0.606
IP Combo	7.866	−34.9	0.234	3.845	0.173
ES Combo*	9.861	−40.0	0.782	6.922	0.713
ED Combo*	7.602	−32.9	0.915	3.786	0.684
Average	8.77 ± 0.93	−36.1 ± 3.5	0.819	5.17 ± 1.47	0.641
Quadratic: N = 2					
IP SOG	0.489	−7.43	0.112	0.444	0.111
ES SOG	0.536	−7.38	0.872	0.501	0.869
ED SOG	0.489	−7.45	0.805	0.443	0.798
ES IFC*	0.497	−5.17	0.875	0.469	0.872
ED IFC*	0.479	−6.90	0.894	0.423	0.882
IP Combo	0.468	−6.23	0.263	0.410	0.259
ES Combo*	0.537	−7.52	0.898	0.502	0.894
ED Combo*	0.451	−5.13	0.988	0.401	0.976
Average	0.491 ± 0.036	−6.18 ± 1.22	0.914	0.449 ± 0.045	0.904
Cubic: N = 3					
IP SOG	0.027	11.57	0.118	0.032	0.115
ES SOG	0.029	8.68	0.893	0.032	0.888
ED SOG	0.027	11.28	0.850	0.032	0.828
ES IFC*	0.029	6.31	0.899	0.031	0.895
ED IFC*	0.030	5.16	0.917	0.033	0.910
IP Combo	0.030	4.67	0.268	0.033	0.266
ES Combo*	0.030	5.48	0.918	0.032	0.916
ED Combo*	0.029	4.78	0.990	0.033	0.980
Average	0.029 ± 0.001	5.42 ± 0.65	0.931	0.032 ± 0.001	0.925

[a]IP SOG, individual points from the SO GasEx data (Figure 7, top); ES SOG, equally spaced wind speed bins using SO GasEx data (Figure 7, bottom); ED SOG, equally distributed bins using SO GasEx data (not shown); ES IFC, equally spaced wind speed bins for the individual field campaigns (Figure 8, bottom); ED IFC, equally distributed bins for the individual field campaigns (not shown); IP Combo, individual points from the combined data (Figure 8, top); ES Combo, equally spaced wind speed bins using the combined data (Figure 9, top); ED Combo, equally distributed bins using the combined data (Figure 9, bottom). The averages are derived from the coefficients denoted by asterisks.

molecular diffusion and turbulence in COAREG is given along with total transfer velocity (i.e., the sum of this component and the bubble mediated exchange). The comparison shows similar results between the transfer velocities derived by the dual tracer and total COAREG algorithm for wind speeds below 10 m s^{-1}. This is to be expected as the COAREG algorithm was tuned to the direct covariance results, which are also in good agreement at these wind speeds. However, it is more informative to compare the 2 components of the COAREG algorithm with the dual tracer results. The dual tracer estimates are approximately twice the molecular/turbulent component in all 3 cases. If the physical processes parameterized in COAREG are correct, this suggests that the gases used in the dual tracer approach are enhanced by bubble mediated exchange.

[58] The transfer velocity estimates obtained by the dual-tracer technique during the 4 day period of highest wind speeds, however, are lower than the COAREG estimate by roughly a factor of 2. It is also lower than the direct covariance based transfer velocities shown in Figure 10 that are used to tune the COAREG algorithm. As such, it can be argued that bubble-mediated exchange impacts the exchange of $^3He/SF_6$ differently than CO_2 at high winds. However, it should also be pointed out that the coefficients that provide the best fit for CO_2 decrease the agreement between COAREG and the transfer velocity for DMS based on direct covariance measurements (see *Fairall et al.* [2011], who assign a turbulent/molecular coefficient of $A = 1.6$ and bubble-mediated coefficient of $B = 1.8$). Therefore, a basic understanding of the processes that govern bubble-mediated exchange for different gases is far from complete.

[59] While the direct covariance approach is expected to give the most direct estimate of the flux, it is clear that individual estimates have significant uncertainty due to all of the issues described above. Averaging reduces the scatter but cannot be expected to remove systematic errors. However, the good agreement between the bin averages from GasEx98 results (based on the closed path sensor) and the SO GasEx

Table 3. Comparison of Dual Tracer and COAREG Transfer Velocities During SO GasEx

	$\overline{U_{10N}}$ (m s^{-1})			Enhancement	K_{660} (cm h^{-1}) Enhancement Corrected		
Period (YD)	Mean	Range	SD	$\overline{U_{10N}^2}/\overline{U_{10N}}^2$	COAREG Mole/Turb	COAREG Total	Dual Tracer
70.20–74.09	8.9	3.9–14.3	1.7	1.04	12.5	27.5	23.7
82.12–86.56	11.2	3.1–16.4	2.8	1.06	14.8	49.9	27.1
86.56–96.03	8.2	1.5–14.6	2.8	1.11	10.9	24.5	18.0

results (based on the open path) shown in Figure 9 is encouraging. These findings are also supported by the good agreement between this study and that by *Prytherch et al.* [2010b]. Therefore, these results argue for significant enhancement of CO_2 at high winds.

[60] It is worth ending this discussion with a brief overview of lessons learned from the three GasEx experiments in our attempts to directly measure the CO_2 fluxes. The setup used in GasEx98 produced transfer velocities with the greatest certainty. The main attribute of this setup was a frequently calibrated closed path NDIR with a short sampling tube and constant flow rate, a flow reservoir to reduce pressure fluctuations, an inline heat exchanger to reduce the Webb correction required for temperature fluctuations, and frequently replaced Gelman filters to remove particles. Therefore, an obvious choice for a future gas exchange experiment would be a similar setup with a closed path NDIRs that can be placed near the sonic anemometer. This may become easier with commercially available equivalents of our shrouded system. However, laboratory and field tests are required to determine whether these systems are better able to reduce the humidity cross talk. It is also worth considering recently developed sensors that rely on cavity ringdown spectroscopy, which appear to be less sensitive to moisture contamination (see Appendix A). Additionally, systems that physically dry the air before it is sampled by the NDIRs may be advantageous even if they require longer sampling tubes.

[61] This experiment also supports the findings of *Miller et al.* [2010] that a significant portion of the motion induced signal comes hydrostatic pressure fluctuations driven by heave. Based on this analysis, the pressure fluctuations estimated from the DCFS heave estimates are able to remove most of this signal in our open path sensors. However, an accurate fast response pressure sensor would be a good addition to any system. This would also provide another means to estimate heave, which can be used as a check on the DCFS estimates of heave and platform velocity. Additionally, accurate inline pressure sensors are necessary for closed path systems to directly remove this signal.

[62] Finally, the success of the GasEx programs stems in large part from the interdisciplinary team of scientist that brought a number of difference approaches to the table. However, the optimal sampling strategy for each approach is sometime at odds with each other. For example, the dual-tracer method requires flexibility in the ship track to optimize sampling of the tracer patch. This results in frequent course changes and often poor relative wind directions. The direct covariance method works best when the ship is pointing into the wind on station or cruising slowly into the wind. This gives the best exposure for the sensors above the bow of the ship, reduces the required motion correction, and reduces the soot contamination from the ship's exhaust. On a typical GasEx cruise, these conditions were met roughly half the time. Therefore, it would be advantageous to the direct covariance teams to conduct an experiment where the ship operations are under their control.

6. Conclusion

[63] Quadratic and cubic wind speed–dependent fits to the CO_2 transfer velocity both give high goodness of fit values with the data after bin averaging. As such, the functionality of the wind speed dependence cannot be unequivocally determined from SO GasEx results. However, the statistics of the various fits favor a cubic over quadratic fit based on the data collected using the direct covariance technique from the three GasEx experiments. As expected, the cubic fit is in good agreement with the study by *McGillis et al.* [2001a], which was based on the GasEx 98 data. However, it is also in good agreement with a recently conducted investigation reported by *Prytherch et al.* [2010b]. The coefficient required to provide the high goodness of fit with the quadratic relationship is also significantly higher than those commonly reported in the literature. To a large extent, this is due to disagreement between the transfer velocities found from the dual tracer approach and those computed using the direct covariance method. The disagreement could be due to either physical processes (e.g., bubble mediated exchange) that may drive real differences between the transfer of CO_2 and the gases used in the dual tracer technique, or due to as yet to be resolved errors in either method. In the case of the direct covariance technique, the majority of the motion induced signal appears arises from hydrostatic pressure perturbations driven by vertical displacement (i.e., heave). However, the exact cause of the humidity cross talk in the open-based NDIRs remains unknown. Nonetheless, the good agreement between the bin-averaged results using significantly different techniques in GasEx 98 and SO GasEx, and between these results and the investigation by *Prytherch et al.* [2010b] verifies that the exchange of CO_2 is significantly enhanced by bubble mediated exchange at high winds.

Appendix A: Water Vapor Contamination of LiCor CO_2 Signal

[64] Implementation of our cross-correlation method to correct for humidity cross talk requires an estimate of the actual cross correlation of humidity and CO_2 associated with surface driven turbulent exchange, which is the second term in the numerator of (19). The flux and the crosstalk coefficient are first rewritten in terms of the specific humidity and let $c = r_c$ for notational convenience

$$\overline{w'c'} = \overline{w'c'_m} - \mu\overline{w'q'} \tag{A1}$$

$$\mu = \frac{\overline{q'c'_m} - \overline{q'c'}}{\sigma_q^2} \tag{A2}$$

where the actual cross correlation is now given by $\overline{q'c'}$. MOST is used to estimate the flux terms

$$\overline{q'c'} = r_{qc}|q_*||c_*|f_\sigma(z/L)^2 \tag{A3a}$$

$$\frac{\sigma_c}{|c_*|} = \frac{\sigma_q}{|q_*|} = f_\sigma(z/L) \tag{A3b}$$

where r_{qc} is an expected humidity-CO_2 correlation coefficient (absolute value near 1.0), x_* are the usual scaling parameters

$$x_* = -\overline{w'x'}/u_* \tag{A4}$$

and f_σ (z/L) is the dimensionless function that accounts for modulation of the scalar standard deviation due to atmospheric stability [*Rowe et al.*, 2011]

$$\begin{aligned} f_\sigma(z/L) &= 3.2 && z/L > 0; \\ f_\sigma(z/L) &= 3.2(1 - 28z/L)^{-1/3} && z/L <= 0; \end{aligned} \tag{A5}$$

where z is the reference height and L is the Obukhov length scale. The height at which $z = -L$ represents the level at which the generation of turbulence due to shear equals the generation of turbulence due to buoyancy. Shear production dominates below this level and buoyant production dominates above.

[65] This simple set of relations offers a number of possibilities for application. For example, values of fluxes and variances can be computed directly from the time series or estimated from the COAREG model. Expression (A3) and (A4) are used in (A2) to obtain

$$\mu = \frac{\overline{q' c_m'}}{\sigma_q^2} - |r_{qr}| \frac{\overline{w'c'}}{\overline{w'q'}} \tag{A6}$$

[66] *Prytherch et al.* [2010a] initially set $\overline{w'c'} = 0$, used (A6) to compute μ, and iterated between (A1) and (A6) until convergence. An alternative to the iterative approach that uses the measured w', q', c_m' sample, is to use (A6) with the second term computed using the COAREG model [*Fairall et al.*, 2000]:

$$|r_{qc}| \frac{\overline{w'c'}}{\overline{w'q'}} = \frac{|r_{qc}| \alpha_c k \Delta f_c C_E S \Delta q f_\sigma(z/L)^2}{u_*^2 \sigma_q^2} = \frac{|r_{qc}| \alpha_c k \Delta f_r}{C_E S \Delta q} \tag{A7}$$

[67] There are two possibilities shown in (A7). The middle term uses the similarity function for the scalar standard deviation and is divided by u_*^2 and the measured σ_q^2, while the last term is restricted to simple bulk variables. The advantage of the bulk approach is that the results are not subject to artificial correlation.

[68] The development so far deals with single humidity cross-talk correction coefficient applied on a segment of data (say, 30 min). In principle, the spectral methods can be used to compute a correction that depends on frequency. The rationale is that the crosstalk effect involves optical surface contaminants that react with fluctuations in humidity and there may be some frequency dependence associated with the reaction time constants.

[69] The spectral equivalents of (A1) and (A2) are given by (20) and (21) above. As with the time series approach, the spectral form of the second term in (21) rewritten here as

$$\mu(\omega) = \frac{C_{qcm}(\omega)}{S_{qc}(\omega)} - \frac{C_{qc}(\omega)}{S_{qq}(\omega)} = \mu_{ccm}(\omega) - \mu_{cc}(\omega) \tag{A8}$$

must be determined to use this approximation. To do this, the spectral form of the correlation coefficient is used:

$$R_{qc}(\omega) = \frac{C_{qc}(\omega) * C_{qc}(\omega)}{S_{qq} S_{cc}} \tag{A9}$$

[70] Thus, the second term in (A8) can be written

$$\frac{C_{qc}(\omega)}{S_{qq}(\omega)} = \sqrt{\frac{R_{qc}(\omega) S_{cc}(\omega)}{S_{qq}(\omega)}} \cong \sqrt{R_{qc}(\omega)} \frac{\overline{w'c'}}{\overline{w'q'}} \tag{A10}$$

where the final term follows from the assumption that the variance spectra are similar.

[71] Expression (17) can be written as

$$c' = c_m' - \mu q' \tag{A11}$$

[72] If both sides of this equation are squared, then an expression relating the *variance spectra* is given by

$$S_{cc}(\omega) = S_{cmcm}(\omega) - \mu(\omega)\left[C_{qcm}(\omega) + C_{qc}(\omega)\right] \tag{A12}$$

[73] The form of the spectral correlation coefficient is easily determined from high-quality fast measurements of temperature and humidity. An example time series from a recent field program is shown in Figure A1 where the sea-air temperature and humidity differences were large enough to place the measurements of temperature and humidity fluctuations well above the instrument noise levels (i.e., assuming that the measurements have no artificial cross talk). The 1 h time series was processed for the variance spectra and the q-T cospectrum (Figure A2) and the spectral correlation coefficient (Figure A3). A simple fit to the correlation in the form

$$R_{qT}(\omega) = \frac{A}{\sqrt{2\pi}\sigma_{\ln}} \exp\left[-\frac{(\ln(\omega) - \ln(0.05 u_{rel}/z))^2}{2\sigma_{\ln}^2} \right] \tag{A13}$$

is shown in Figure A3 where $A = 5.5$, $\sigma_{\ln} = 2.5$, u_{rel} is the relative wind speed, and z is the height of the observation. If the model for R_{qT} given by (A13) is combined with S_{qq} and S_{TT} (replacing S_{cc}) in (A10), then the second term in (A8) is reproduced as shown in Figure A4.

[74] Some sample time series obtained from an independent deployment during the CalNex experiment are examined to test the corrections in the spectral domain. One CO_2 time series comes from a LI-7500 that has been washed with clean, fresh water twice a day. As in the above analysis, water vapor dilution correction has been made to the time series using the LI-7500 fast q values, and the temperature dilution correction has been made using the fast air temperature derived from the sonic anemometer. The other CO_2 time series from a Picarro 2000 system, which has water vapor removed via Nafion filter. The Picarro was located in the lab and is sampling through a 75 m tube, which induces a 21 s delay that has been accounted for in processing. Examples of processing for $\mu(\omega)$ in the spectral domain are shown in Figure A5. For these two examples $\mu(\omega)$ is about 4 over most of the frequency domain. The raw LiCor w-CO_2 cospectrum shows substantial humidity contamination in Figure A6. However, the corrected cospectrum agrees well with the Picarro.

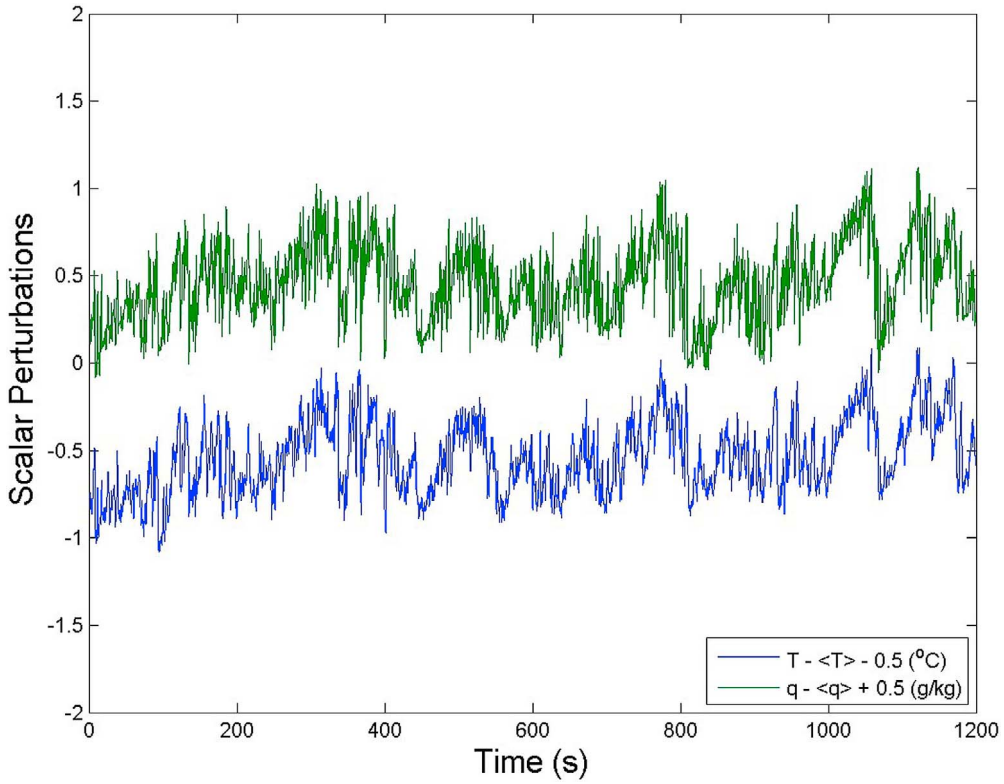

Figure A1. Time series of detrended specific humidity (green) and temperature (blue) at 19 m over the ocean, 1000 GMT, 23 May 2010, off the coast of Los Angeles, California. The sea-air temperature difference is 3.1 C, and the wind speed is 10.4 m s^{-1}.

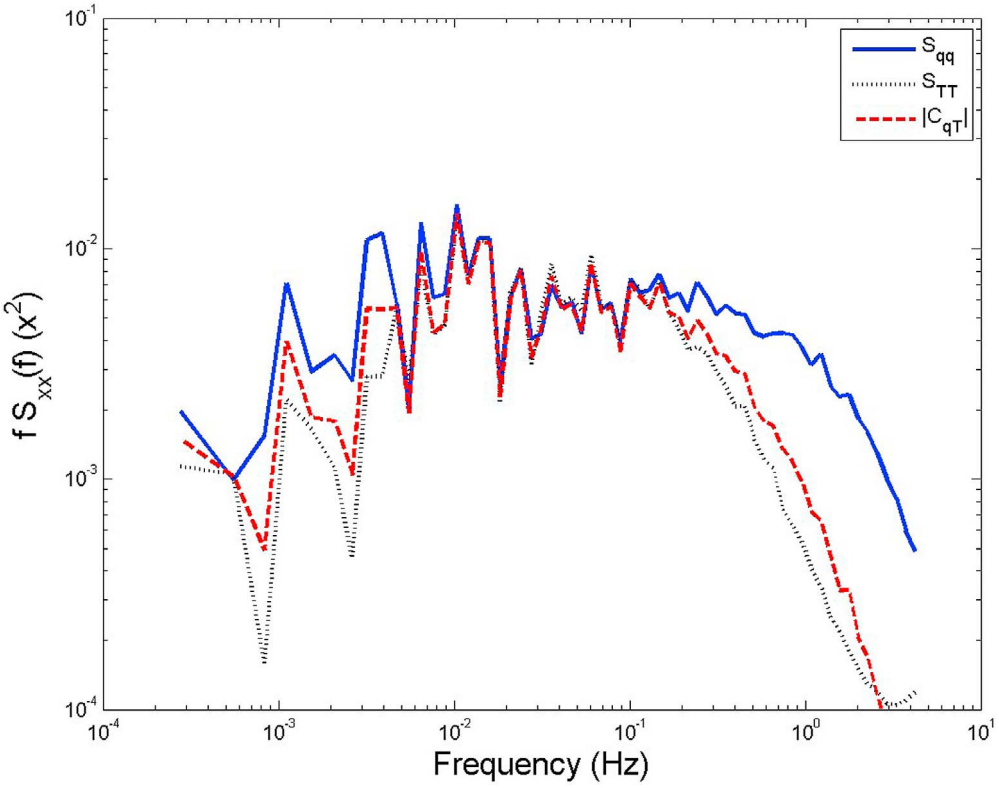

Figure A2. Variance spectra for humidity (blue line) and temperature (dotted line) and the q-T cospectrum (red dashed line) for the time series shown in Figure A1.

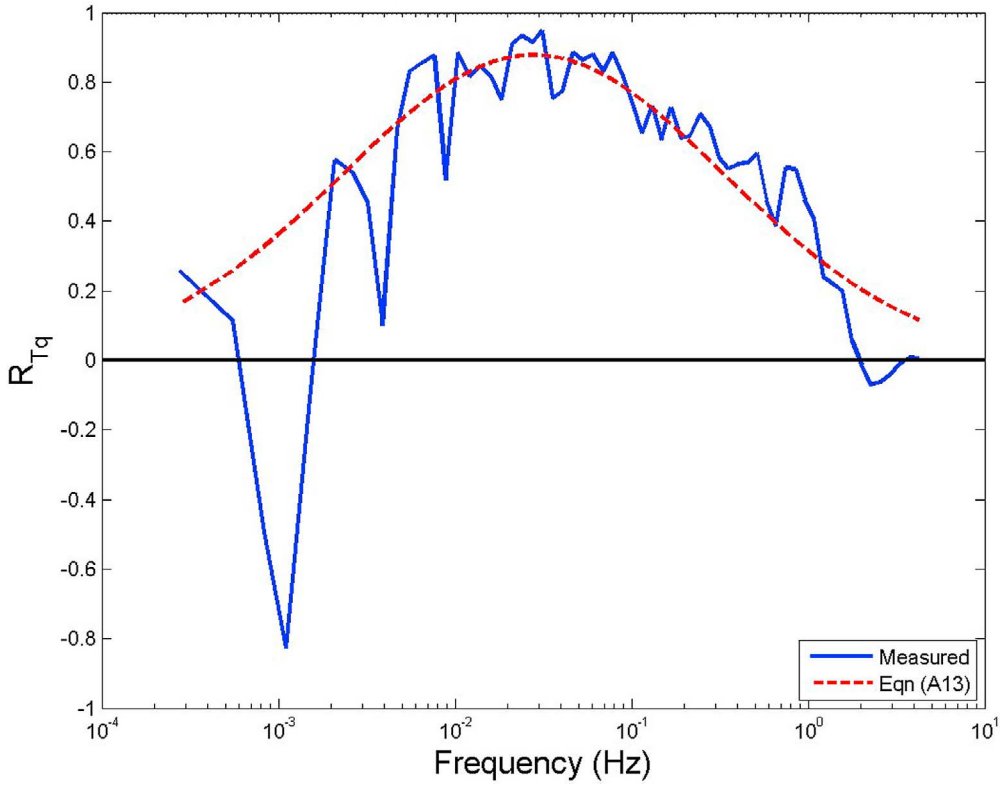

Figure A3. Spectral correlation coefficient for temperature-humidity from the 1 h time series in Figure A1.

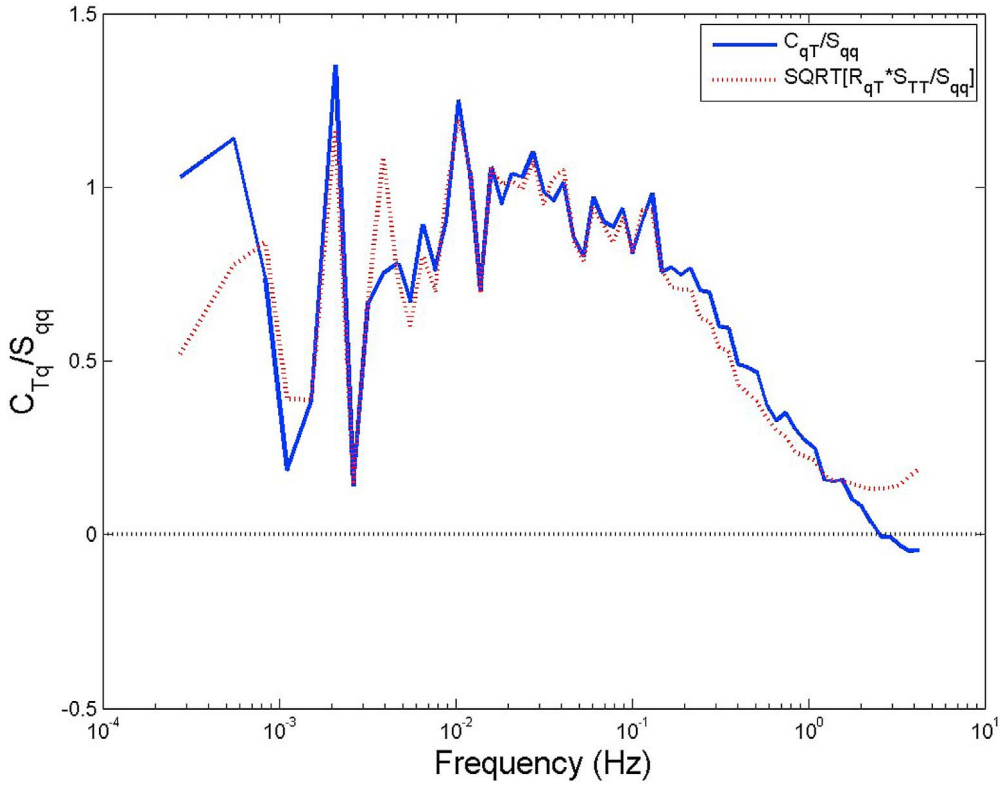

Figure A4. The frequency-dependent real atmospheric correlation factor (second term in (A8)). The blue line is the direct observation; the dotted red line uses (A13) in (A10).

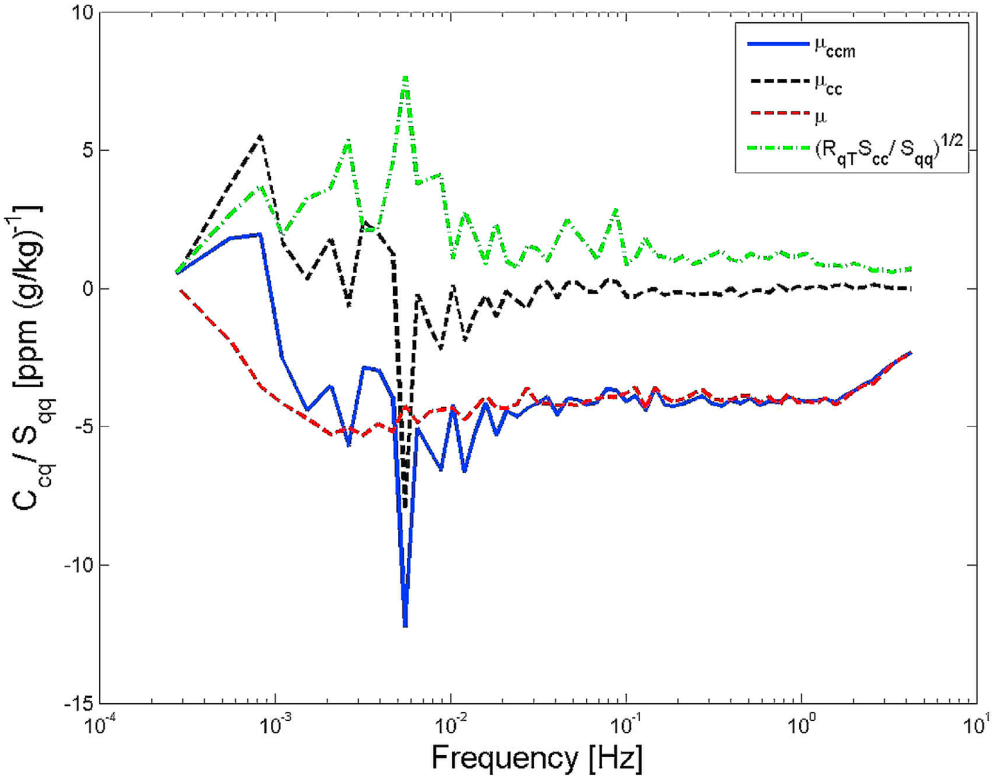

Figure A5. Spectral correction factors versus frequency for 23 May at 1300 GMT. The first term in (A8), μ_{ccm}, is shown as the blue line; the second term in (A8), μ_{cc}, is the dotted blue line; μ_{cc} estimated with (A13) is the dotted green line; and $\mu = \mu_{ccm} - \mu_{cc}$ is the dashed red line. Note that because the humidity cross talk is anticorrelated, a negative sign is required with the square root term for μ_{cc}.

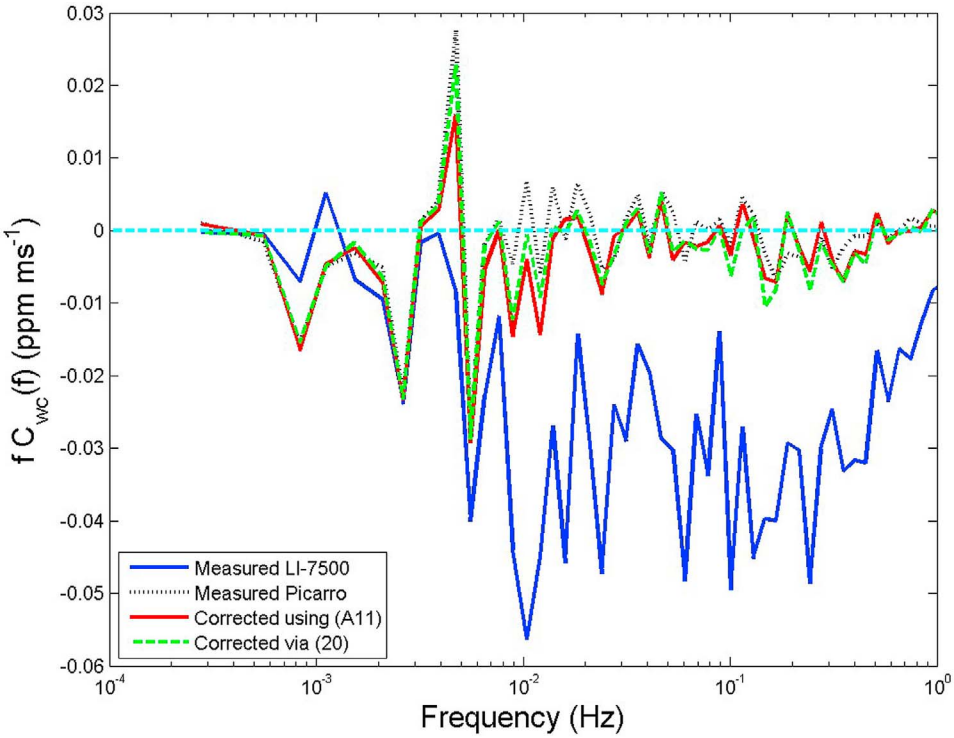

Figure A6. The w-c cospectra versus frequency corresponding to Figure A5. The raw LI-7500 w-c cospectrum is in blue, the Picarro 2000 w-c cospectrum is the dotted blue line, the cospectrum derived from the $c' = c'_m - \mu q'$ time series is in red, and the corrected spectrum as per (20) is the dashed green line.

[75] **Acknowledgments.** This material is based upon work supported by the National Science Foundation under grant 0647475, the National Oceanic and Atmospheric Administration under grant NA07OAR4310084, and the NOAA Office of Climate Observations.

References

Bariteau, L., J. Hueber, K. Lang, D. Helmig, C. W. Fairall, and J. E. Hare (2010), Ozone deposition velocity by ship-based eddy correlation flux measurements, *Atmos. Meas. Tech.*, *3*, 441–455, doi:10.5194/amt-3-441-2010.

Blomquist, B. W., C. W. Fairall, B. Huebert, and D. J. Kleiber (2006), DMS sea-air transfer velocity: Direct measurements by eddy covariance and parameterization based on the NOAA/COARE Gas Transfer Model, *Geophys. Res. Lett.*, *33*, L07601, doi:10.1029/2006GL025735.

Blomquist, B. W., B. J. Huebert, C. W. Fairall, and I. C. Faloona (2010), Determining the sea-air flux of dimethylsulfide by eddy correlation using mass spectrometry, *Atmos. Meas. Tech.*, *3*, 1–20, doi:10.5194/amt-3-1-2010.

Broadgate, W. (Ed.) (2004), SOLAS science plan and implementation strategy, *IGBP Rep.*, *50*, 88 pp., IGBP Secr., Stockholm.

Businger, J. A. (1997), On the measurement of the transfer of gases across the air-sea interface, *J. Appl. Meteorol.*, *36*, 1113–1115, doi:10.1175/1520-0450(1997)036<1113:OTMOTT>2.0.CO;2.

Dickson, A. G., C. L. Sabine, and J. R. Christian (Eds.) (2007), *Guide to Best Practices for Ocean CO_2 Measurements*, *PICES Spec. Publ.*, *3*, 191 pp., N. Pac. Mar. Sci. Organ., Sydney, B. C., Canada.

Dupuis, H., C. Guerin, D. Hauser, A. Weill, P. Nacass, W. M. Drennan, S. Cloche, and H. C. Graber (2003), Impact of flow distortion corrections on turbulent fluxes estimated by the inertial dissipation method during the FETCH experiment on R/V *L'Atalante*, *J. Geophys. Res.*, *108*(C3), 8064, doi:10.1029/2001JC001075.

Edson, J. B., and C. W. Fairall (1998), Similarity relationships in the marine atmospheric surface layer for terms in the TKE and scalar variance budgets, *J. Atmos. Sci.*, *55*, 2311–2328, doi:10.1175/1520-0469(1998)055<2311:SRITMA>2.0.CO;2.

Edson, J. B., A. A. Hinton, K. E. Prada, J. E. Hare, and C. W. Fairall (1998), Direct covariance flux estimates from mobile platforms at sea, *J. Atmos. Oceanic Technol.*, *15*, 547–562, doi:10.1175/1520-0426(1998)015<0547:DCFEFM>2.0.CO;2.

Edson, J. B., C. J. Zappa, J. A. Ware, W. R. McGillis, and J. E. Hare (2004), Scalar flux profile relationships over the open ocean, *J. Geophys. Res.*, *109*, C08S09, doi:10.1029/2003JC001960.

Edson, J. B., M. D. DeGrandpre, N. Frew, and W. R. McGillis (2008), Investigations of air-sea gas exchange in the CoOP coastal air-sea chemical flux program, *Oceanography*, *21*, 34–45.

Fairall, C. W., E. F. Bradley, J. S. Godfrey, J. B. Edson, G. S. Young, and G. A. Wick (1996a), Cool skin and warm layer effects on the sea surface temperature, *J. Geophys. Res.*, *101*, 1295–1308, doi:10.1029/95JC03190.

Fairall, C. W., E. F. Bradley, D. P. Rogers, J. B. Edson, and G. S. Young (1996b), Bulk parameterization of air-sea fluxes for TOGA COARE, *J. Geophys. Res.*, *101*, 3747–3764, doi:10.1029/95JC03205.

Fairall, C. W., J. E. Hare, J. B. Edson, and W. McGillis (2000), Parameterization and micrometeorological measurements of air-sea gas transfer, *Boundary Layer Meteorol.*, *96*, 63–106, doi:10.1023/A:1002662826020.

Fairall, C. W., E. F. Bradley, J. E. Hare, A. A. Grachev, and J. B. Edson (2003), Bulk parameterization of air-sea fluxes: Updates and verification for the COARE algorithm, *J. Clim.*, *16*, 571–591, doi:10.1175/1520-0442(2003)016<0571:BPOASF>2.0.CO;2.

Fairall, C. W., L. Bariteau, A. A. Grachev, R. J. Hill, D. E. Wolfe, W. Brewer, S. Tucker, J. E. Hare, and W. Angevine (2006), Coastal effects on turbulent bulk transfer coefficients and ozone deposition velocity in ICARTT, *J. Geophys. Res.*, *111*, D23S20, doi:10.1029/2006JD007597.

Fairall, C. W., J. E. Hare, D. Helmig, and L. Ganzveld (2007), Water-side turbulence enhancement of ozone deposition to the ocean, Atmos. *Chem. Phys.*, *7*, 443–451, doi:10.5194/acp-7-443-2007.

Fairall, C. W., M. Yang, L. Bariteau, J. B. Edson, E. Helmig, W. McGillis, W. Pezoa, J. E. Hare, B. Huebert, and B. Blomquist (2011), Implementation of the Coupled Ocean-Atmosphere Response Experiment flux algorithm with CO_2, dimethyl sulfide, and O_3, *J. Geophys. Res.*, *116*, C00F09, doi:10.1029/2010JC006884.

Hare, J., C. Fairall, W. McGillis, J. Edson, B. Ward, and R. Wanninkhof (2004), Evaluation of the NOAA/COARE air-sea gas transfer parameterization using GasEx data, *J. Geophys. Res.*, *109*, C08S02, doi:10.1029/2003JC002256.

Hintsa, E. J., J. W. H. Dacey, W. R. McGillis, J. B. Edson, C. J. Zappa, and H. J. Zemmelink (2004), Sea-to-air fluxes from measurements of the atmospheric gradient of dimethylsulfide and comparison with simultaneous relaxed eddy accumulation measurements, *J. Geophys. Res.*, *109*, C01026, doi:10.1029/2002JC001617.

Ho, D. T., C. S. Law, M. J. Smith, P. Schlosser, M. Harvey, and P. Hill (2006), Measurements of air-sea gas exchange at high wind speeds in the Southern Ocean: Implications for global parameterizations, *Geophys. Res. Lett.*, *33*, L16611, doi:10.1029/2006GL026817.

Ho, D. T., C. L. Sabine, D. Hebert, D. S. Ullman, R. Wanninkhof, R. C. Hamme, P. G. Strutton, B. Hales, J. B. Edson, and B. R. Hargreaves (2011a), Southern Ocean Gas Exchange Experiment: Setting the stage, *J. Geophys. Res.*, *116*, C00F08, doi:10.1029/2010JC006852.

Ho, D. T., R. Wanninkhof, P. Schlosser, D. S. Ullman, D. Hebert, and K. F. Sullivan (2011b), Toward a universal relationship between wind speed and gas exchange: Gas transfer velocities measured with 3He/SF6 during the Southern Ocean Gas Exchange Experiment, *J. Geophys. Res.*, *116*, C00F04, doi:10.1029/2010JC006854.

Kohsiek, W. (2000), Water vapor cross-sensitivity of open-path H_2O/CO_2 sensors, *J. Atmos. Oceanic Technol.*, *17*, 299–311, doi:10.1175/1520-0426(2000)017<0299:WVCSOO>2.0.CO;2.

Kondo, F., and O. Tsukamoto (2007), Air-sea CO_2 flux by eddy covariance technique in the equatorial Indian Ocean, *J. Oceanogr.*, *63*, 449–456, doi:10.1007/s10872-007-0040-7.

Lauvset, S. K., W. R. McGillis, L. Bariteau, C. W. Fairall, T. Johannessen, A. Olsen, and C. J. Zappa (2011), Direct measurements of CO_2 flux in the Greenland Sea, *Geophys. Res. Lett.*, *38*, L12603, doi:10.1029/2011GL047722.

Liss, P. S., and L. Merlivat (1986), Air-sea gas exchange rates: Introduction and synthesis, in *The Role of Air-Sea Interactions in Geochemical Cycling*, edited by P. Buat-Menard, pp. 113–129, D. Reidel, Hingham, Mass.

Liss, P. S., and P. G. Slater (1974), Flux of gases across the air-sea interface, *Nature*, *247*, 181–184, doi:10.1038/247181a0.

MacIntyre, S., W. Eugster, and G. W. Kling (2001), The critical importance of buoyancy flux for gas flux across the air-water interface, in *Gas Transfer at Water Surfaces*, *Geophys. Monogr. Ser.*, vol. 127, edited by M. A. Donelan et al., pp. 135–139, AGU, Washington, D. C.

Marandino, C., W. De Bruyn, S. Miller, and E. Saltzman (2009), Eddy correlation measurements of the air/sea flux of dimethylsulfide over the Eastern Pacific Ocean, *Atmos. Chem. Phys.*, *9*, 345–356, doi:10.5194/acp-9-345-2009.

McGillis, W. R., and R. Wanninkhof (2006), Aqueous CO_2 gradients for air-sea flux estimates, *Mar. Chem.*, *98*, 100–108, doi:10.1016/j.marchem.2005.09.003.

McGillis, W. R., J. W. H. Dacey, N. M. Frew, E. J. Bock, and B. K. Nelson (2000), Water-side flux of dimethylsulfide, *J. Geophys. Res.*, *105*, 1187–1193, doi:10.1029/1999JC900243.

McGillis, W. R., J. B. Edson, J. E. Hare, and C. W. Fairall (2001a), Direct covariance air-sea CO_2 fluxes, *J. Geophys. Res.*, *106*, 16,729–16,745, doi:10.1029/2000JC000506.

McGillis, W. R., J. B. Edson, J. D. Ware, J. W. H. Dacey, J. E. Hare, C. W. Fairall, and R. Wanninkhof (2001b), Carbon dioxide flux techniques performed during GasEx-98, *Mar. Chem.*, *75*, 267–280, doi:10.1016/S0304-4203(01)00042-1.

McGillis, W. R., J. B. Edson, C. J. Zappa, E. Terray, J. E. Hare, C. W. Fairall, W. M. Drennan, and M. A. Donelan (2004), Air-sea CO_2 fluxes in the equatorial Pacific, *J. Geophys. Res.*, *109*, C08S02, doi:10.1029/2003JC002256.

Miller, S., C. Marandino, W. de Bruyn, and E. S. Saltzman (2009), Air-sea gas exchange of CO_2 and DMS in the North Atlantic by eddy covariance, *Geophys. Res. Lett.*, *36*, L15816, doi:10.1029/2009GL038907.

Miller, S. D., C. Marandino, and E. S. Saltzman (2010), Ship-based measurement of air-sea CO_2 exchange by eddy covariance, *J. Geophys. Res.*, *115*, D02304, doi:10.1029/2009JD012193.

Naegler, T. P., P. Ciais, K. Rodgers, and I. Levin (2006), Excess radiocarbon constraints on air-sea gas exchange and the uptake of CO_2 by the oceans, *Geophys. Res. Lett.*, *33*, L11802, doi:10.1029/2005GL025408.

Nightingale, P. D., G. Malin, C. S. Law, A. J. Watson, P. S. Liss, M. J. Liddicoat, J. Boutin, and R. C. Upstill-Goddard (2000), In situ evaluation of air-sea gas exchange using novel conservative and volatile tracers, *Global Biogeochem. Cycles*, *14*, 373–387, doi:10.1029/1999GB900091.

Prytherch, J., M. J. Yelland, R. W. Pascal, B. I. Moat, I. Skjelvan, and C. C. Neill (2010a), Direct measurements of CO_2 flux over the ocean: Development of a novel method, *Geophys. Res. Lett.*, *37*, L03607, doi:10.1029/2009GL041482.

Prytherch, J., M. J. Yelland, R. W. Pascal, B. I. Moat, I. Skjelvan, and M. A. Srokosz (2010b), Open ocean gas transfer velocity derived from long-term direct measurements of CO_2 flux, *Geophys. Res. Lett.*, *37*, L23607, doi:10.1029/2010GL045597.

Rowe, M. D., C. W. Fairall, and J. A. Perlinger (2011), Chemical sensor resolution requirements for near-surface measurements of turbulent fluxes, *Atmos. Chem. Phys.*, *11*, 5263–5275, doi:10.5194/acp-11-5263-2011.

Rutgersson, A., A. Smedman, and E. Sahlée (2011), Oceanic convective mixing and the impact on air-sea gas transfer velocity, *Geophys. Res. Lett.*, *38*, L02602, doi:10.1029/2010GL045581.

Soloviev, A. V. (2007), Coupled renewal model of ocean viscous sublayer, thermal skin effect and interfacial gas transfer velocity, *J. Mar. Syst.*, *66*, 19–27, doi:10.1016/j.jmarsys.2006.03.024.

Soloviev, A. V., and P. Schlüssel (1994), Parameterization of the cool skin of the ocean and of the air-ocean gas transfer on the basis of modeling surface renewal, *J. Phys. Oceanogr.*, *24*, 1339–1346, doi:10.1175/1520-0485(1994)024<1339:POTCSO>2.0.CO;2.

Takahashi, T., J. Olafsson, J. Goddard, D. W. Chipman, and S. C. Sutherland (1993), Seasonal variation of CO_2 and nutrients in the high-latitude surface oceans: A comparative study, *Global Biogeochem. Cycles*, *7*, 843–878, doi:10.1029/93GB02263.

Taylor, P. K. (2000), Intercomparison and validation of ocean–atmosphere energy flux fields, final report of the Joint WCRP/SCOR Working Group on Air-Sea Fluxes, *Rep. WCRP-112*, 306 pp., World Clim. Res. Programme, Geneva, Switzerland.

U.S. Department of Energy (1994), Handbook of methods for the analysis of the various parameters of the carbon dioxide system in sea water, version 2, *Rep. ORNL/CDIAC-74*, edited by A. G. Dickson and C. Goyet, Washington, D. C.

Vlahos, P., and E. C. Monahan (2009), A generalized model for the air-sea transfer of dimethylsulfide at high wind speeds, *Geophys. Res. Lett.*, *36*, L21605, doi:10.1029/2009GL040695.

Wanninkhof, R. (1992), Relationship between wind speed and gas exchange over the ocean, *J. Geophys. Res.*, *97*, 7373–7382, doi:10.1029/92JC00188.

Wanninkhof, R., and M. Knox (1996), Chemical enhancement of CO_2 exchange in natural waters, *Limnol. Oceanogr.*, *41*, 689–697, doi:10.4319/lo.1996.41.4.0689.

Wanninkhof, R., and W. R. McGillis (1999), A cubic relationship between air-sea CO_2 exchange and wind speed, *Geophys. Res. Lett.*, *26*, 1889–1892, doi:10.1029/1999GL900363.

Wanninkhof, R., W. E. Asher, D. T. Ho, C. Sweeney, and W. R. McGillis (2009), Advances in quantifying air-sea gas exchange and environmental forcing, *Annu. Rev. Mar. Sci.*, *1*, 213–244, doi:10.1146/annurev.marine.010908.163742.

Webb, E. D., G. I. Pearman, and R. Leuning (1980), Correction of flux measurements for density due to heat and water vapor transport, *Q. J. R. Meteorol. Soc.*, *106*, 85–100, doi:10.1002/qj.49710644707.

Weiss, R. F. (1970), The solubility of nitrogen, oxygen and argon in water and seawater, *Deep Sea Res.*, *17*(4), 721–735.

Weiss, R. F. (1974), Carbon dioxide in water and seawater: The solubility of a non-ideal gas, *Mar. Chem.*, *2*, 203–215, doi:10.1016/0304-4203(74)90015-2.

Woolf, D. K. (1997), Bubbles and their role in gas exchange, in *The Sea Surface and Global Change*, edited by R. Duce, P. Liss, and U. Cambridge, pp. 173–206, Cambridge Univ. Press, Cambridge, U. K., doi:10.1017/CBO9780511525025.007.

Yang, M., B. W. Blomquist, C. W. Fairall, S. D. Archer, and B. J. Huebert (2011), Air-sea exchange of dimethylsulfide in the Southern Ocean: Measurements from SO GasEx compared to temperate and tropical regions, *J. Geophys. Res.*, *116*, C00F05, doi:10.1029/2010JC006526.

Zemmelink, H. J., J. W. H. Dacey, E. J. Hintsa, W. R. McGillis, W. W. C. Gieskes, W. Klaassen, H. W. de Groot, and H. J. W. de Baar (2004), Fluxes and gas transfer rates of the biogenic trace gas DMS derived from atmospheric gradients, *J. Geophys. Res.*, *109*, C08S10, doi:10.1029/2003JC001795.

L. Bariteau and J. E. Hare, Cooperative Institute for Research in Environmental Sciences, University of Colorado at Boulder, Boulder, CO 80309, USA.

A. Cifuentes-Lorenzen and J. B. Edson, Department of Marine Sciences, University of Connecticut, Groton, CT 06340, USA. (james.edson@uconn.edu)

C. W. Fairall and S. Pezoa, Earth System Research Laboratory, NOAA, Boulder, CO 80305, USA.

D. Helmig, Institute of Alpine and Arctic Research, University of Colorado at Boulder, Boulder, CO 80309, USA.

W. R. McGillis and C. J. Zappa, Lamont-Doherty Earth Observatory, Earth Institute at Columbia University, Palisades, NY 10964, USA.